Scientific Reports

https://doi.org/10.1038/s41598-026-62932-2

Article in Press

Effects of pulse-type near-fault ground motions on the nonlinear seismic response of steel frames with inverted-V CBF and EBF systems

Received: 18 May 2026

Accepted: 15 July 2026

Published online: 23 July 2026

Cite this article as: Yurdakul M., Tonyali Z., Sesli H. *et al.* Effects of pulse-type near-fault ground motions on the nonlinear seismic response of steel frames with inverted-V CBF and EBF systems. *Sci Rep* (2026). https://doi.org/10.1038/s41598-026-62932-2

Muhammet Yurdakul, Zeliha Tonyali, Hasan Sesli & Maziar Fahimi Farzam

We are providing an unedited version of this manuscript to give early access to its findings. Before final publication, the manuscript will undergo further editing. Please note there may be errors present which affect the content, and all legal disclaimers apply.

If this paper is publishing under a Transparent Peer Review model then Peer Review reports will publish with the final article.

ARTICLE IN PRESS

© The Author(s) 2026. **Open Access** This article is licensed under a Creative Commons Attribution-NonCommercial-NoDerivatives 4.0 International License, which permits any non-commercial use, sharing, distribution and reproduction in any medium or format, as long as you give appropriate credit to the original author(s) and the source, provide a link to the Creative Commons licence, and indicate if you modified the licensed material. You do not have permission under this licence to share adapted material derived from this article or parts of it. The images or other third party material in this article are included in the article's Creative Commons licence, unless indicated otherwise in a credit line to the material. If material is not included in the article's Creative Commons licence and your intended use is not permitted by statutory regulation or exceeds the permitted use, you will need to obtain permission directly from the copyright holder. To view a copy of this licence, visit http://creativecommons.org/licenses/by-nc-nd/4.0/.

ARTICLE IN PRESS

Effects of Pulse-Type Near-Fault Ground Motions on the Nonlinear Seismic Response of Steel Frames with Inverted-V CBF and EBF Systems

Muhammet Yurdakul[1], Zeliha Tonyali[2*], Hasan Sesli[3], Maziar Fahimi Farzam[4,5]

[1] Department of Civil Engineering, The Faculty of Technology, Karadeniz Technical University, Trabzon, Turkey
[2] Department of Civil Engineering, The Faculty of Engineering and Architecture, Recep Tayyip Erdogan University, Rize, 53100, Turkey
[3]Department of Civil Engineering, The Faculty of Engineering, Yalova University, Yalova, Turkey
[4]Department of Civil Engineering, University of Maragheh, East Azarbaijan, Maragheh 83111-5518, Iran.
[5]Sahand University of Technology, Faculty of Civil Engineering, Tabriz, Iran
* Corresponding author: Zeliha Tonyali (**e-mail**:zeliha.tonyali@erdogan.edu.tr)

Abstract

The type of lateral load-resisting system plays a critical role in controlling the seismic response of steel structures subjected to strong ground motions. In this research, the structural performance of three-dimensional (3D) steel buildings designed with concentrically braced frames (CBFs) and eccentrically braced frames (EBFs) under near-fault ground excitations (NFGEs). A 3D steel building with dual bracing systems, including inverted-V-shaped EBFs and CBFs, were designed under the influence of NFGE. The response of 4 and 8-story structures subjected to NFGE was assessed using nonlinear time history analyses (NTHAs), which were categorized into small-pulse (SP), medium-pulse (MP), and large-pulse (LP) scenarios. This research aims to assess how pulse characteristics affect lateral story and inter-story displacements in buildings of different heights, as these displacement demands are critical indicators of seismic performance and structural strength degradation. This study provides a systematic evaluation of the seismic response of low- and mid-rise CBF and EBF systems under different pulse-type near-fault ground motions, highlighting the role of lateral story displacements as a key performance indicator. The results demonstrate that seismic performance is highly dependent on building height and pulse characteristics, with EBFs showing superior performance in mid-rise buildings under medium-pulse excitations, while CBFs are more effective in low-rise structures, emphasizing the need for height- and pulse-specific bracing strategies.

ARTICLE IN PRESS

Keywords: Concentrically braced frames (CBFs), Eccentrically braced frames (EBFs), Inverted-V bracing, steel frames, Near-fault seismic excitation, Pulse effects, Shear and axial hinges

1. Introduction

The dynamic behavior of steel structural systems under seismic loading has been a critical research topic in earthquake engineering, particularly for structures employing bracing systems to enhance lateral stiffness and seismic resilience. Steel braced frames are widely used due to their efficiency in resisting seismic base shear, where inelastic behavior is intentionally concentrated in specific structural components while the remaining members are designed to remain essentially elastic [1]. Among these systems, concentrically braced frames (CBFs) and eccentrically braced frames (EBFs) are two of the most commonly adopted configurations in earthquake-resistant design, each offering distinct advantages and limitations that have been extensively discussed in the literature [2-6]. According to the Turkish Building Earthquake Code (TBEC 2018) [7], typical brace configurations for CBFs and EBFs are illustrated in **Figure 1**.

CBFs are characterized by their truss-like behavior, in which braces align with beams and columns to provide high lateral stiffness and strength. Despite their structural simplicity and effectiveness in resisting

ARTICLE IN PRESS

lateral loads, CBFs are prone to brittle brace buckling and fracture under severe cyclic loading, which may lead to significant strength degradation and potential collapse [8]. In contrast, EBFs combine the favorable stiffness characteristics of braced frames with the ductility of moment-resisting frames (MRFs) by introducing eccentricity in brace connections. This configuration enables improved seismic performance through controlled energy dissipation, reduced force transmission to primary structural members, and greater architectural flexibility [9, 10]. Consequently, EBFs have been shown to outperform CBFs in terms of ductility and seismic energy dissipation, particularly under strong ground motions.

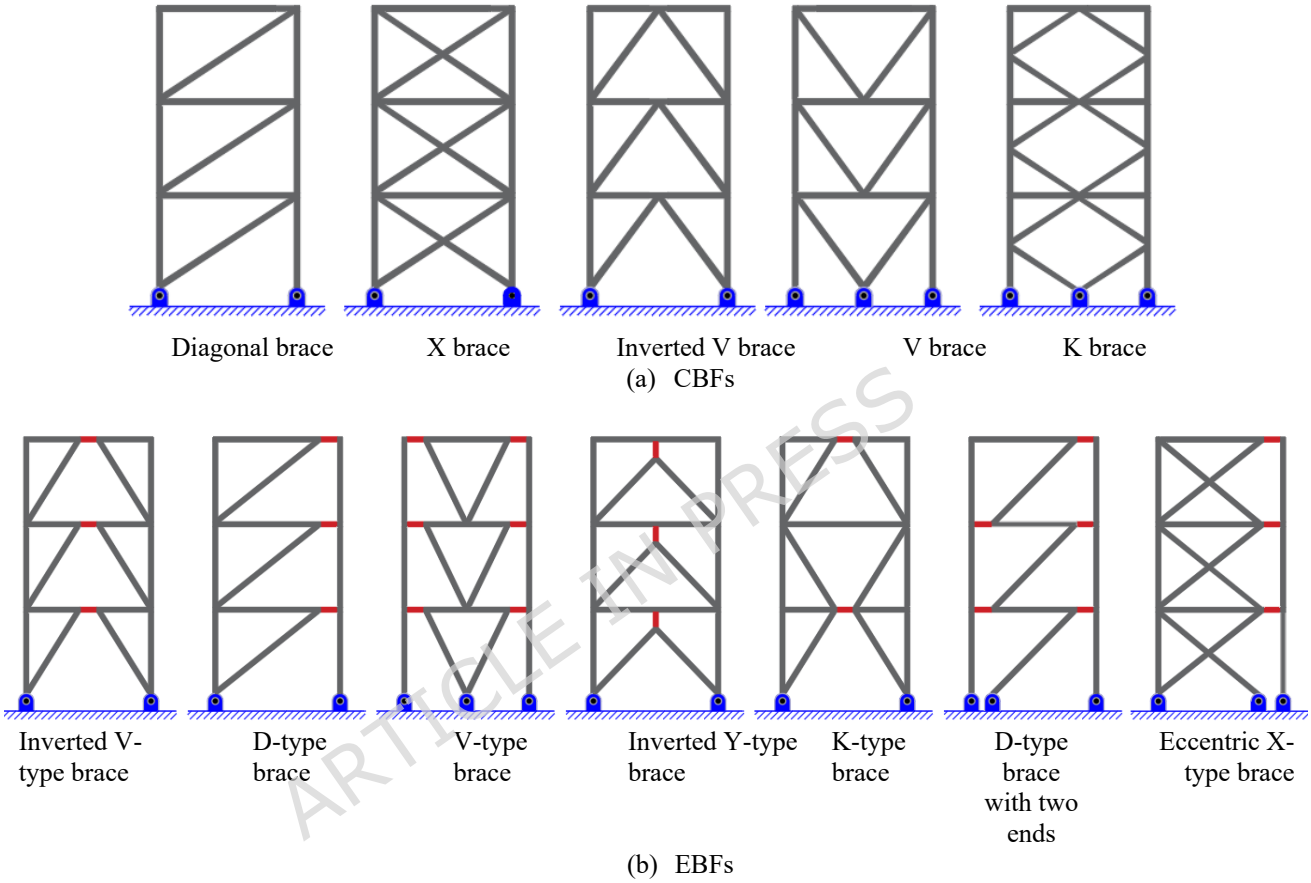


Figure 1. Brace configuration of (a) CBFs, (b) EBFs according to TBEC 2018 code (adapted from [7])

In EBF systems, seismic energy dissipation is intentionally concentrated in short beam segments known as link elements, which are designed to undergo controlled yielding in shear, flexure, or a combination of both [11, 12]. According to Eurocode 8 [13], plastic deformations should be confined to the link elements, while braces, columns, and beam segments outside the links are expected to remain essentially elastic. A defining characteristic of EBFs is that axial forces induced by the braces are transferred to adjacent members primarily through shear and bending actions in the link segment. The global stiffness and seismic response of EBFs are therefore highly dependent on the link length-to- the span length ratio (e/L). When the link length approaches the span length (e=L), the system behaves similarly to an MRF with relatively low stiffness, whereas decreasing the link length (e) increases stiffness of the EBFs, reaching its maximum when the link length is zero (i.e., e=0), which is equivalent to a CBFs configuration [14]. However, excessively short links must still be capable of sustaining large cyclic deformations without premature failure, necessitating careful balance between stiffness and ductility.

ARTICLE IN PRESS

The seismic performance of EBFs has been extensively investigated through experimental and numerical studies focusing on link behavior, deformation mechanisms, and design optimization. Prior research has demonstrated that short links provide stable hysteretic behavior, enhanced drift capacity, and improved fatigue resistance [15-18]. Previous research on EBF link beams has demonstrated that their seismic performance is strongly governed by link type, detailing, and axial force demands. Okazaki and Engelhardt [19] showed that shear-dominated links are prone to web fracture, particularly when modern rolled sections are used, leading to the need for revised flange slenderness limits and improved detailing. Richards and Uang [20] confirmed that maintaining adequate web slenderness and flange strength is essential for achieving stable and ductile cyclic behavior in short links. Focusing on reliability, Mojarad and Daei [21] found that while short links generally meet target safety levels under seismic loading, longer links exhibit reduced reliability due to high axial force effects, indicating the necessity for design modification factors. Manganiello et al. [22] proposed empirical formulations for evaluating the overstrength and rotation capacity of short links under axial constraints, while Almasabha [23] reported that current AISC seismic provisions [24] may underestimate the plastic shear strength of short links. More recently, numerical and data-driven approaches have been employed to assess the influence of additional system components, such as masonry infill walls, on the seismic response of EBFs [25]. Tonyali [10] examined the seismic response of short-link EBFs subjected to pulse-type ground motions by implementing a Uniform Damage Distribution (UDD) design approach through story-wise variation of shear link cross-sections. NTHAs demonstrated that the UDD-based design significantly reduces inter-story drift demands and displacement responses, confines inelastic deformations within IO–LS performance levels, and promotes a more uniform distribution of hysteretic energy dissipation under strong velocity pulses. Collectively, these studies emphasize the critical role of the link element in governing the global seismic behavior of EBF systems.

In addition to structural configuration, the characteristics of earthquake ground motions significantly influence seismic response. NFGEs are typically characterized by pulse-like velocity demands occurring early in the shaking, resulting in substantial energy input and amplified structural response [26, 27]. Conversely, FFGEs, although generally associated with lower velocity amplitudes, can still induce significant structural damage due to their longer duration and cumulative energy input, particularly in medium- to high-rise buildings [28]. Differences between near-fault (NF) and far-fault (FF) ground motions are influenced by several factors, including earthquake magnitude, rupture mechanism, source depth, distance to the fault, and local site conditions [29, 30]. To better characterize pulse-like ground motions, near-fault records are commonly classified based on pulse period into SP, MP, and LP categories. Each pulse category imposes distinct demands on structural systems. SPs, characterized by rapid velocity changes, can induce high stress concentrations and localized damage, potentially exceeding elastic limits [31-33]. MPs involve a combination of low- and high-frequency content, often leading to complex structural responses such as increased lateral displacements and torsional effects [34-36]. LPs, commonly associated with large-magnitude or distant earthquakes, predominantly affect flexible structures, such as high-rise buildings, where responses are governed by fundamental vibration modes and may result in large global displacements [37, 38].

Recent studies have further demonstrated that the seismic performance of CBF and EBF systems is strongly dependent on building height, bracing configuration, and the adopted energy dissipation mechanism. The studies on CBFs subjected to NFGEs have reported complex dynamic responses, including concentration of damage in weaker stories and heightened collapse probability under fault-normal pulse

ARTICLE IN PRESS

components [39-42]. Many of these investigations focused on limited building heights, single-story systems, or did not explicitly distinguish between pulse-period categories. In contrast, EBFs offer a hybrid structural solution capable of enhancing both ductility and energy dissipation through controlled yielding of link elements, thereby delaying brace buckling and preserving global stability under severe seismic demands [43-45]. Comparative investigations indicate that EBFs generally exhibit reduced story displacement demands and enhanced energy dissipation capacity compared to CBFs under similar seismic loading conditions, particularly in mid- to high-rise structures, owing to their ability to accommodate inelastic deformations through link yielding [46]. Parametric and performance-based studies on multi-story steel frames retrofitted with various bracing systems have shown that while CBFs are more effective in low-rise buildings, EBFs configurations provide superior damage mitigation and ductility in taller structures [47, 48]. Additional numerical and experimental studies have highlighted that brace eccentricity, link configuration, and brace typology significantly influence stiffness, displacement control, and energy dissipation characteristics, leading to distinct damage mechanisms in CBF and EBF systems [49, 50]. Under NFGEs, EBFs have been reported to outperform CBFs in terms of controlled inelastic behavior, reduced lateral displacements, and improved achievement of target yield mechanisms, particularly when forward-directivity effects are considered within performance-based design frameworks [45, 51]. Moreover, investigations on composite systems subjected to both NF and FF ground motions have confirmed that damage is predominantly concentrated in link elements, with its extent governed by link length and building height, while overall drift demands are significantly reduced through the inclusion of bracing systems [52]. More recent studies on advanced steel frame systems have also emphasized that residual drift mitigation, self-centering capability, and enhanced post-yield stiffness are critical performance objectives for modern braced steel frames [53-55] Despite these advances, a systematic comparison of CBF and EBF systems under pulse-type NFGEs, explicitly accounting for pulse-period characteristics across different building heights, remains limited.

The present study investigates the seismic response demands of 3D low- and mid-rise steel buildings equipped with dual lateral load-resisting systems consisting of inverted V-shaped CBFs or EBFs combined with MRFs. The main objective is to comparatively evaluate the response of 4- and 8-story CBF and EBF systems under the selected NFGEs categorized according to pulse period as SP, MP, and LP records. Previous studies have examined the seismic behavior of CBFs and EBFs under NFGEs; however, a systematic comparison of inverted V-shaped CBF and EBF systems across different building heights while explicitly considering pulse-period categories remains limited. In particular, the combined influence of building height, bracing-system mechanism, and pulse-period characteristics on lateral displacement, inter-story drift, brace/link performance, and force–displacement response has not been sufficiently clarified. Building upon the findings of Tonyali et al. [40], who reported that inverted V-shaped bracing provided a favorable response among different CBF configurations under NFGEs, the present study extends the investigation by directly comparing inverted V-shaped CBF and EBF systems in 3D steel buildings. The novelty of this study lies in its height-dependent and pulse-period-based assessment of CBF and EBF response mechanisms under selected NFGEs. Unlike previous studies that generally focused on a single bracing system, limited building heights, or NFGEs without explicitly distinguishing SP, MP, and LP pulse categories, this study evaluates how the interaction between pulse characteristics and structural configuration affects global and local seismic response demands. The specific contributions of this study are as follows: (i) a comparative nonlinear dynamic assessment of 4- and 8-story inverted V-shaped CBF and EBF systems under SP, MP, and LP near-fault pulse records; (ii) evaluation of height-dependent displacement and inter-story drift demand trends for the two bracing systems; (iii) interpretation of the

ARTICLE IN PRESS

observed response differences in terms of structural stiffness, pulse-to-structure period interaction, velocity-pulse intensity, effective momentum transfer, brace yielding/buckling, and link yielding mechanisms; and (iv) identification of record-dependent response trends that clarify the limitations of attributing seismic response demands to pulse duration alone.

2. Material and Method

2.1. Near Fault Ground Excitations (NFGEs)

Earthquakes are inevitable natural phenomena that pose significant hazards due to the uncertainty associated with their occurrence. Consequently, a thorough consideration of ground excitations (GEs) is essential for mitigating earthquake risk through effective urban planning, safer structural design, and improved understanding of their potential impact on structures. In this context, the characteristics of ground motion play a more critical role in governing structural response than earthquake magnitude alone. The seismic response of a structure is governed by both structural parameters (i.e., mass, natural period, damping, and stiffness) and ground-motion characteristics (i.e., amplitude, duration, and frequency content).

GEs are classified in earthquake engineering according to the distance between the fault and the damaged region. The two primary GEs categories, which are essential to the design of earthquake-resistant structures and the assessment of seismic hazards, are FFGEs and NFGEs. These categories enable the construction of more resilient buildings by revealing the various seismic wave forms and their effects on structures. In these excitations, as seismic waves pass through the Earth's crust, they lose a significant amount of their intensity, resulting in more distributed, lower energy shaking in these places. Also, it affects a greater region and can nevertheless provide serious threats to structures, especially those that are susceptible to long-duration shaking, even though it often results in less severe ground acceleration than NFGE. FFGEs tend to show longer and more complex waveforms, although their velocity pulses are less noticeable [56]. As for NFGEs, which are known as the GMs that occur near the fault of the earthquake, they take place within 20 km of the rupture ($R_{rup} \leq 20km$) [57, 58]. This type of GM is characterized by intense shaking over a short period, often with a significant velocity pulse. This pulse-like excitation occurs when seismic waves are focused in the direction of fault rupture. NFGEs can generate large displacements and velocities that place extreme demands on buildings and infrastructure, especially those with longer natural periods. In addition, these excitations with large velocity pulses bring about high seismic demands for structures. The unique features of NFGEs, such as high energy concentration and directional effects, make them a critical consideration for structures located near active fault zones [59, 60].

In structural earthquake design, large-amplitude coherent pulses, which are usually identified in the velocity time histories, are a common characteristic of earthquake GMs recorded at a close distance to the fault. These coherent pulses, which are generally lacking in typical FFGEs, are strongly influenced by the tectonic movement-induced permanent ground displacement at the site as well as the rupture mechanism and slip direction relative to the site [40, 61]. Compared to FFGEs, velocity pulses exhibit a long period and short duration, resulting in noticeably stronger seismic responses [62, 63]. In NF locations, these short and strong pulses are the main sources of structural damage. Pulse-like records are well recognized for their potential to impose higher demands on structures when compared with ordinary records [64].

Pulse like GMs (i.e, forward-directivity, or the fling-step effects) often have enormous amplitudes and are focused in a narrow-band frequency region. These excitations are characterized by a distinct, large intensity velocity pulse at the beginning of time-history records. Nevertheless, not every NFGE is pulse-

ARTICLE IN PRESS

type, and some may not even exhibit pulse-like features [65]. As a consequence, pulse effects produce uncommon response spectral shapes, with an amplified bump in the medium- to long-period range that is centered near the pulse period (T_P) [66-68]. Also, it is generally accepted that the pulses are the result of either the fling-step effects (FSEs) or the forward-directivity effects (FDEs) [65], depending on the characteristics of the earthquake source, the location of the recording station with respect to the fault rupture, and the site conditions. However, recent research [69, 70] has shown that the pulses may be impacted simultaneously by both the FSEs and the FDEs. The FSEs happens the consequence of a fault rupture that leads to a permanent displacement of the ground during seismic GMs. Whereas the FDEs take place when the fault ruptures in the direction of the site at a speed about equivalent to the shear wave velocity (V_{s30}) [71]. Also, FDE does not produce any permanent ground displacement and hence two-sided velocity pulses. As a result, the wavefront arrives as a single, massive pulse in FDEs [65].

NFGE is defined by specific characteristics that distinguish it from other types of seismic activity, primarily due to its proximity to the seismic fault. Various studies have outlined different criteria to identify and classify NFGE. Some of the main criteria are proximity to the fault, velocity pulses, GM's duration and amplitude, and directivity effect [72]. NFGEs typically occur within $R_{rup} \leq 20km$ of the fault and are characterized by high-intensity shaking and velocity pulses [57, 58, 73]. The ratio of peak ground velocity (PGV) to peak ground acceleration (PGA) must be greater than 0.10 s, and the velocity pulse duration must be greater than 1.0 s [74]. Besides these, T_p/T_1 is a critical number which is a ratio of the pulse duration to the first mode period for specifying the structural response under NFGEs with pulse. Although GMs with long T_p/T_1 have larger mode effects and maximum reaction at higher stories, the short period structures under the records with a large pulse have a maximum ductility demand in bottom stories [40, 75, 76]

In the present study, 4- and 8-story CBF and EBF systems were analyzed under NFGEs exhibiting different pulse durations. The pulse period (T_p) is identified as the time needed to complete a full velocity cycle and is obtained in the velocity time histories (VTHs) of the selected ground excitations. The duration of the extracted pulse period is considered by selecting a proper NFGE, and selected excitations are also classified sets as LP, MP, and SP, as shown in **Table 1**. The large, medium, and small pulse periods are respectively over 3 s., a range of about 1.5 s. and about 2.9 s., and smaller than about 1.2 s. Besides, every record set given in **Table 1**, which contained three types of NFGE, is nearly the same PGV/PGA.

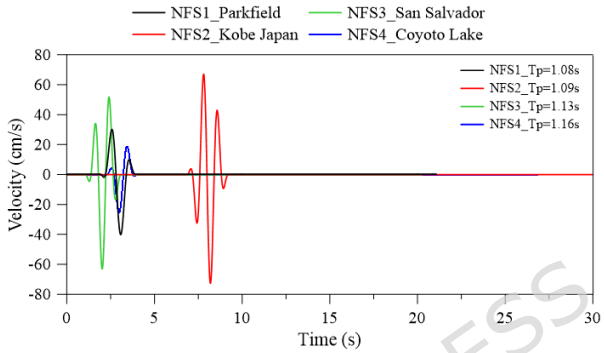
Table 1 Dynamic characteristics of NFGEs considered in the study [77]

Excitation Type		*RSN*	*Earthquake*	M_w	R_{rup} *(km)*	PGA *(g)*	PGV *(cm/s)*	$\frac{PGV}{PGA}(s)$	T_P *(s)*
*NFS**	NFS1	4100	Parkfield-02, CA	6.00	3.01	0.373	44.80	0.12	1.08
	NFS2	1106	Kobe, Japan	6.90	0.96	0.630	76.11	0.12	1.09
	NFS3	569	San Salvador	5.80	6.99	0.534	72.99	0.14	1.13
	NFS4	148	Coyote Lake	5.74	7.42	0.256	29.58	0.12	1.16
*NFM**	NFM1	1013	Northridge-01	6.69	5.92	0.324	47.38	0.15	1.62
	NFM2	1119	Kobe, Japan	6.90	0.27	0.614	86.25	0.14	1.81
	NFM3	723	Superstition Hills-02	6.54	0.95	0.384	53.06	0.14	2.39
	NFM4	828	Cape Mendocino	7.01	8.18	0.662	88.51	0.14	2.99
*NFL**	NFL1	1085	Northridge-01	6.69	5.19	0.449	60.41	0.14	3.53
	NFL2	802	Loma Prieta	6.93	8.50	0.326	45.97	0.14	4.57
	NFL3	1165	Kocaeli, Turkey	7.51	7.21	0.165	22.33	0.14	5.37
	NFL4	143	Tabas, Iran	7.35	2.05	0.862	123.4	0.15	6.19

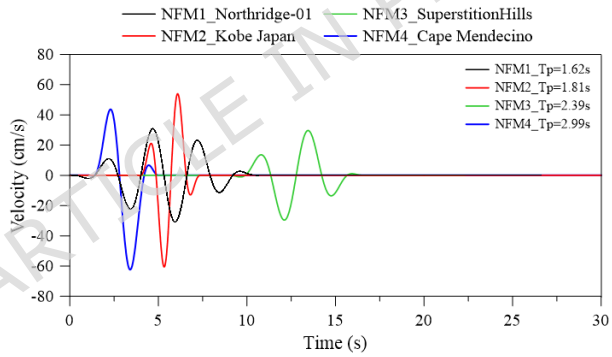
NFS NF ground excitations (small-pulse period)*
NFM NF ground excitations (medium-pulse period)*
NFL NF ground excitations (large-pulse period)*

ARTICLE IN PRESS

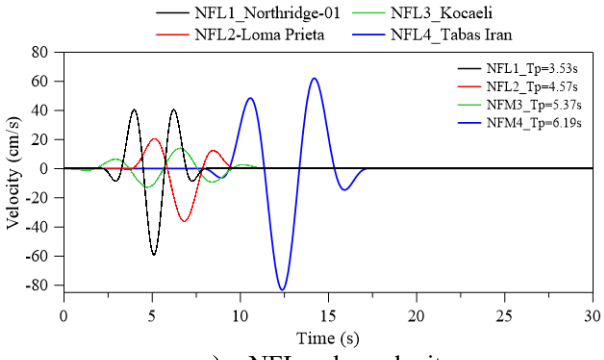
In addition, the VTHs of GMs with the associated extracted pulses for small, medium, and large pulse periods of selected excitations are given in **Figure 2**. The pulse velocities associated with selected excitations are drawn using SeismoSignal [78] software according to the method proposed by Kardoutsou et el. [79]. Overall, **Figure 2** clearly demonstrates that pulse period significantly influences both the timing and duration of velocity demand imposed on structures. While NFS motions concentrate velocity demand early and over short durations, NFL motions impose sustained velocity pulses that control the response of flexible systems. NFM motions represent a transitional behavior between these two extremes. This clear distinction justifies the classification of the selected ground motions into SP, MP and LP categories and highlights the necessity of explicitly considering pulse period effects when evaluating the seismic performance of CBF and EBF systems



a) NFS pulse velocity



b) NFM pulse velocity



c) NFL pulse velocity

Figure 2 Pulse velocity graphics of the selected excitations, a) NFS, b) NFM, and c) NFL pulses

ARTICLE IN PRESS

2.2. Nonlinear Material Behavior and Structural Properties

To investigate the nonlinear characteristics of 3D steel buildings with CBFs and EBFs, nonlinear modeling techniques were employed. These models account for material and geometric nonlinearity to accurately simulate the complex behavior of steel bracing systems in nonlinear dynamic analyses. The 3D nonlinear modeling was performed using SAP2000 software. The material used in this research is the S355 steel, widely used in the construction field due to its good strength characteristics as well as good welding properties, and its material properties is given in **Table 2**. The stress-strain curve of the material used in the non-linear analyses was drawn in **Figure 3**. The CBFs and EBFs were modelled with a multilinear material model characterized by a yield strength of 355 MPa, an elastic modulus of 210 GPa, and 1.5% post-yield strain hardening. NTHAs were performed to evaluate the response of low-rise, and mid-rise structures subjected to NFGEs, incorporating the influence of SP, MP, and LP ground motions. P-Delta effects were incorporated in the analysis to account for the interaction between axial forces and lateral displacements in the models. In the NTHAs, a constant damping ratio of 5% was applied uniformly across all vibration modes. This choice reflects the typical level of inherent energy dissipation observed in steel frame structures under dynamic loading conditions, as recommended by seismic design guidelines such as ASCE/SEI 41-17 and Eurocode 8. This approach assumes equal damping for each mode to represent the energy dissipation capacity of the structure under dynamic loading conditions. The study captures critical nonlinear parameters, such as lateral displacement, stiffness degradation, and energy dissipation, to assess the dynamic performance of CBF and EBF systems under varying seismic conditions.

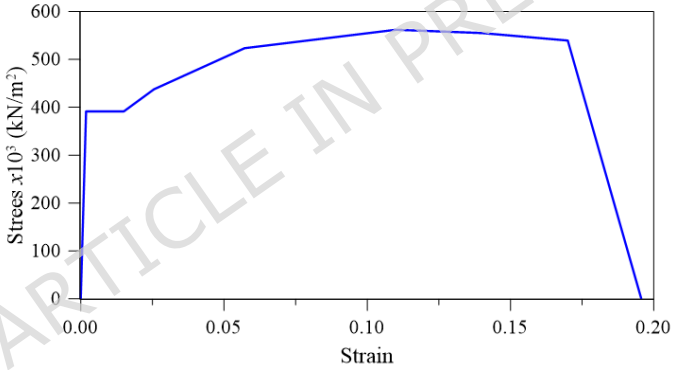


Figure 3 Stress-strain curve of the steel material

Table 2 Material properties of steel

Property		
Steel grade	:	S355
Weight per unit volume (kN/m^3)	:	76.97
Modulus of elasticity (kN/m^2)	:	2.1x10^8
Poisson ratio	:	0.3
Modulus of Shear (kN/m^2)	:	80769231
Minimum yield stress (kN/m^2)	:	355000
Minimum tensile stress (kN/m^2)	:	510000
Directional symmetry type	:	Isotropic
Strain at onset of strain hardening	:	0.015
Strain at maximum stress	:	0.11
Strain at rapture	:	0.17

ARTICLE IN PRESS

2.3. Modelling of the horizontal shear link element

In EBFs, a capacity design approach is adopted to ensure that inelastic deformations are confined exclusively to the shear links, while all other structural members are proportioned to remain essentially elastic under seismic loading. Due to the critical role of the link in energy dissipation, extensive experimental and analytical research has focused on its seismic behavior. One of the main factors influencing an EBF system's stiffness, strength, ductility, and behavior is the link element's length (e). Properly detailed link elements exhibit significant energy dissipation capacity and stable hysteretic behavior under strong ground motions. Moreover, in combination with braces, they provide high lateral stiffness and mitigate damage under low-intensity seismic events [80, 81]. A straightforward way to measure the yield behavior is to use the link element length ratio, which is represented the symbol ρ, and it is calculated by the following formula as $\rho = e/(Mp/Vp)$, where Mp and Vp represent for the link element's plastic bending moment and plastic shear force capabilities, respectively. The inelastic response of a link is strongly influenced by the link length and the Mp/Vp ratio of the link element. [12, 23, 82]. Mp and Vp can be calculated as below:

$$V_p = \frac{F_{yw}}{\sqrt{3}}\, t_w \left(d - 2t_f\right) \quad (1)$$

$$M_p = F_{yf}\, t_f \left(b - t_w\right) \left(d - t_f\right) + \frac{F_{yw}\, t_w\, d^2}{4} \quad (2)$$

where F_{yw} and F_{yf} are the web and flange yield strength, respectively. t_w, t_f, d, b are the web thickness, the flange thickness, the overall beam depth, and the flange width, respectively. Based on the geometric and material properties of the selected section, the plastic shear capacity and plastic moment capacity of the link were calculated as $V_p = 1213kN$ and $M_p = 1596kNm$, respectively.

Previous studies [19, 83] have demonstrated that horizontal beam shear links exhibit excellent ductility and energy dissipation, provided their length is designed to enable shear yielding without web buckling. Significant strain hardening behavior, consistent with an isotropic hardening assumption, was observed together with pronounced bending–shear interaction, leading to enhanced plastic moment and shear capacities of the link elements. At ultimate load, shear and moment capacities reached approximately $1.5Vp$ and $1.2Mp$, respectively. To ensure shear yielding precedes bending yielding, the link length e must be limited [14, 84]:

$$e \le \frac{2 * 1.2M_p}{1.5V_p} = 1.6\frac{M_p}{V_p} \quad (3)$$

The classification is based on the normalized link length (ρ) defined as;

$$\rho = e\frac{V_p}{M_p} \quad (4)$$

Link beams are categorized into three groups: i) short (shear-dominated, $e \le 1.6M_p/V_p$), ii) intermediate (shear-flexural, $1.6M_p/V_p < e < 2.6M_p/V_p$), and iii) long (flexural-dominated, $e \ge 2.6M_p/V_p$). Short shear link are generally preferred due to their enhanced ductility, lateral stiffness, and energy dissipation capacity under seismic loading [23]. The shear links (i.e., $e \le 1.6M_p/V_p$ or $\rho \le 1.6$) have a maximum link rotation of 0.08 rad under the design seismic loading and yield mostly in shear [85]. However, architectural

ARTICLE IN PRESS

constraints often necessitate the use of intermediate and long links in practice [86]. Also, there are substantial differences between the behavior of short and long links. Short links perform significantly better than long links under severe cyclic loading, particularly in terms of strength and ductility, as shown by early experimental studies from Roeder and Popov [14, 87]. Over time, Popov et al. [88] suggested various practical limits for shear-dominated behavior, ultimately determining a limit of $\rho \leq 1.6$, which is still used in design standards such as AISC 341-10 [24].

In this study, the link element of the EBF system is explicitly modeled using nonlinear frame elements. The link length and span length are 1.0 m and 6.0 m, respectively, resulting in a link length to span length ratio (e/L) of 0.17. The corresponding normalized link length ratio (ρ) are obtained as ρ=0.76, which classifies the link as a short (shear-dominated) link according to the AISC 341-10 [24]. This ratio is a critical parameter influencing the seismic performance of EBFs, as it governs the deformation capacity, energy dissipation, and overall lateral stiffness of the system. In the model, to simulate the inelastic response under seismic loading, plastic hinges were assigned in the middle of the link element. These hinges were defined using a shear hinge model (V3 direction), calibrated according to FEMA 356 guideline to represent nonlinear shear behavior. The details of link element's hinge properties are given in **Figure 4**.

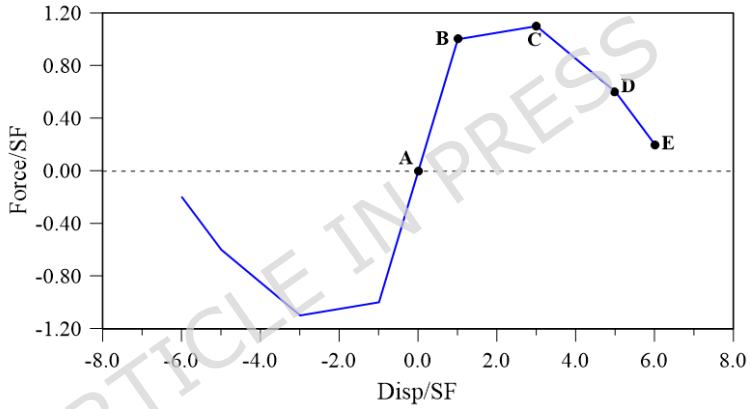


Figure 4. Force-deformation curve of the shear hinge defined for the link beam (adapted from FEMA 356 [89] and AISC [90])

2.4.Modelling of the axial hinge on the brace

In CBF systems designed according to force-based seismic provisions, energy dissipation is primarily achieved through axial yielding of braces in tension and global or local buckling in compression, rather than through the development of stable, distributed ductility mechanisms. Under strong ground motions, braces typically exhibit a highly asymmetric axial force–deformation response characterized by stable yielding in tension and rapid strength degradation following buckling in compression [24, 91]. Accurately capturing this behavior is therefore essential for realistic nonlinear time-history analyses of CBF systems. In this study, the inelastic axial behavior of brace elements was modeled in SAP2000 by assigning axial plastic hinges with user-defined axial force–displacement backbone curves. This curve is presented in normalized form as illustrated in **Figure 5**. The axial force is normalized by the axial yield force of the brace (N_y), while the axial displacement is normalized by the corresponding axial yield displacement (Δ_y). This normalization allows the backbone curve to be defined in a dimensionless form and consistently implemented within the SAP2000 axial plastic hinge framework, independent of the absolute brace size and material strength. To avoid artificial stiffness concentration at member ends and to better represent the

ARTICLE IN PRESS

distributed nature of axial yielding and buckling, the axial hinge was located at the mid-length of each brace member, which is a commonly adopted assumption in nonlinear brace modeling. Similar hinge placement strategies have been employed in previous numerical studies focusing on brace buckling and cyclic degradation [92, 93].

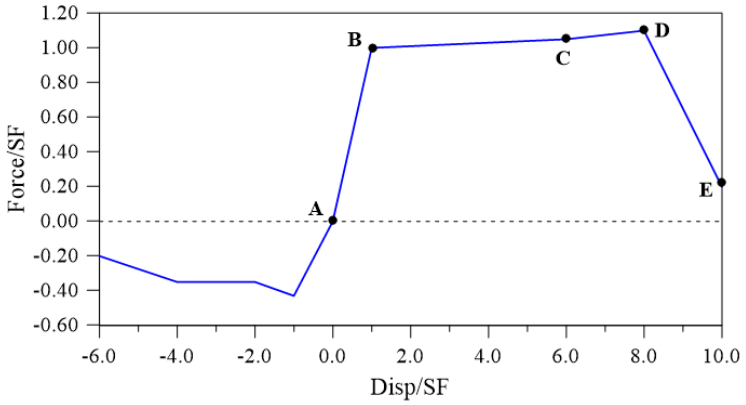


Figure 5 Normalized axial force–displacement backbone curve adopted for brace axial hinge modeling

The axial hinge backbone was defined in terms of normalized axial force and normalized axial displacement, following a piecewise-linear representation consisting of five characteristic points (A–B–C–D–E). The backbone curve was defined independently for tension and compression to reflect the inherent asymmetry of brace behavior. The adopted axial hinge backbone curve is illustrated in **Figure 5**. In this Figure, the positive branch (A–E) represents the tensile behavior of the brace, while the negative branch corresponds to compressive behavior, including buckling and post-buckling strength degradation. The post-buckling residual compressive strength was assumed to be 1050kN, which corresponds to a normalized compressive force level of $1050/N_y$ in the adopted axial backbone curve. The initial elastic stiffness of the brace was defined as:

$$k_{axial} = \frac{EA}{L} \quad (5)$$

where E is the elastic modulus, A is the cross-sectional brace area, and L is the brace length. This stiffness governs the response up to the axial yield point in tension or the critical buckling load in compression. In tension, the axial yield force N_y was calculated as:

$$N_y = A f_y \quad (6)$$

where f_y is the yield stress of the steel material. Beyond yielding, a slight post-yield hardening was introduced to represent material strain hardening, with a hardening ratio on the order of 1–2% of the elastic stiffness. This assumption ensures numerical stability while remaining consistent with experimental observations of steel brace behavior. The post-yield branch was extended until the target deformation capacity was reached, without explicitly modeling fracture, as brace rupture was not the focus of the present study. In compression, brace capacity was governed by elastic buckling. The critical buckling load N_{cr} was calculated using Euler's formula:

$$N_{cr} = \frac{\pi^2 EI}{(KL)^2} \quad (7)$$

where I is the weak-axis moment of inertia and K is the effective length factor. Upon reaching the buckling load, a sudden strength degradation was introduced in the backbone curve to simulate post-buckling

ARTICLE IN PRESS

behavior. Following common practice in nonlinear brace modeling, the residual compressive strength was assumed to drop to a fraction of the peak buckling load and to remain approximately constant at larger compressive deformations [94, 95].

An isotropic hysteretic rule was adopted for the axial hinge to account for stiffness degradation and strength deterioration under cyclic tension–compression loading. Load-carrying capacity beyond the ultimate deformation point (E) was assumed to drop to zero, preventing unrealistically high force transfer at excessive axial deformations. This assumption is consistent with the collapse prevention philosophy adopted in FEMA 356 and ASCE 41. Performance limits corresponding to Immediate Occupancy (IO), Life Safety (LS), and Collapse Prevention (CP) were defined in terms of normalized plastic axial displacement and used exclusively for performance evaluation during post-processing. In SAP2000, the term hinge state refers to the internal force–deformation condition of a plastic hinge (A–B–C–D–E), which directly reflects the progression of inelastic behavior. In contrast, hinge status indicates the performance level (e.g., IO, LS, CP) assigned based on acceptance criteria defined in seismic design and assessment standards, such as ASCE 41, FEMA 356, or similar performance-based guidelines. In this study, interpretations are primarily based on hinge states, as they provide a direct and unambiguous representation of the physical response.

The axial yield displacement of the brace, Δ_y, represents the axial deformation at which yielding initiates under tensile loading and constitutes the reference deformation used to normalize the axial hinge backbone curve. In the present study, the yield displacement was computed based on linear elastic axial deformation theory as:

$$\Delta_y = \frac{N_y L}{AE} \quad (8)$$

where N_y is the axial yield force of the brace, L is the brace length, E is the elastic modulus of brace, and A is the cross-sectional area of brace. The calculated yield displacement was subsequently used as the displacement normalization parameter in the axial hinge definition. Such normalization is consistent with common nonlinear brace modeling practices and facilitates objective comparison of inelastic deformation demands across different brace configurations. By defining the axial hinge backbone in terms of normalized force N/N_y and displacement Δ/Δ_y, the modeling approach avoids dependence on absolute deformation values and ensures scalability of the hinge properties with respect to brace length and section characteristics. The mechanical and geometric properties of the brace members, together with the parameters used for axial hinge definition, are summarized in **Table 3**. The axial hinge backbone curve was derived directly from these quantities, ensuring consistency between section properties, elastic stiffness, axial yield capacity, and buckling behavior. The force–displacement backbone of the axial hinge (**Figure 5**) was constructed by normalizing the axial force and displacement with respect to the yield force N_y and yield displacement Δ_y reported in **Table 3**, while post-buckling degradation in compression was defined based on the buckling ratio and residual strength factor β.

Table 3 Axial hinge modeling parameters adopted for brace elements

Parameter	*Symbol*	*Value*	*Unit*
Brace section	-	IPE400	-
Cross-section	A	0.00846	m^2
Steel yield strength	f_y	355	MPa
Elastic modulus	E	210	GPa
Brace length	L	4.6	m
Weak-axis moment of inertia	I_y	1.318×10^{-5}	m^4

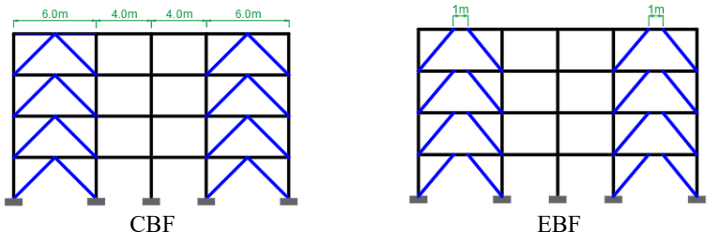
ARTICLE IN PRESS

Axial yield force	N_y	3000	kN
Axial elastic stiffness	k_{axial}	0.3856x10^9	N/m
Yield displacement	Δ_y	7.78	mm
Critical buckling load	N_{cr}	1290	kN
Buckling to yield ratio	N_{cr}/N_y	0.43	-
Post buckling strength factor	β	0.35	-
Residual compressive strength	$N_{pb} = \beta N_y$	1050	kN

The adopted nonlinear modelling strategy was checked and justified by comparing its assumptions with previously published experimental and numerical studies. The steel material model, plastic hinge definitions, brace axial hinge backbone, shear link hinge model, and damping assumptions are consistent with established seismic assessment guidelines and commonly used nonlinear modelling approaches in the literature [89, 90]. In particular, the CBF model captures the expected asymmetric brace response, including tensile yielding, compressive buckling, and post-buckling strength degradation, as reported in previous studies on brace cyclic behavior [96-98]. Similarly, the EBF model concentrates inelastic deformation in the shear link, which is consistent with capacity design principles and previous experimental observations on shear-dominated link behavior [23, 85, 86, 99]. Therefore, the adopted modelling approach is considered suitable for evaluating the comparative nonlinear response trends of the selected CBF and EBF systems.

2.5. Numerical Examples

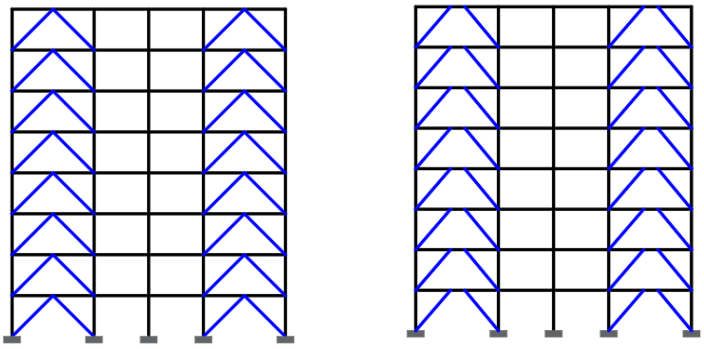
The x-z elevation view of the structural configuration of the analyzed CBF and EBF is illustrated in **Figure 6**. Each building model was developed for two different heights: 4-story (low-rise) and 8-story (mid-rise). Each model has a 4-span in the x-direction and y-direction; the end span length in both directions is 6m, the interior span length is 4m, the first story height is 3.5m, and the other stories' heights are 3m. The story diaphragms are assumed to behave as rigid within their plane. The floors were modelled with rigid diaphragms, assuming that in-plane deformations of the slabs are negligible compared to their out-of-plane flexibility. This rigid diaphragm assumption ensures uniform displacement distribution across the plan for each floor under lateral loading. CBF and EBF configurations were placed in the corner bays of the frames in both the x- and y-directions for both building heights, as shown in **Figure 6**. This placement aims to enhance lateral stiffness and energy dissipation under seismic excitations while minimizing interference with architectural planning. 3D FEM of the CBFs and EBFs models is given in **Figure 7**. The NTHAs were carried out in the 3D numerical models of CBFs and EBFs. Young's modulus of the steel was taken as 2.1×10^5 MPa. The H400×237, H400×593, and IPE400 profile sections were used in the beam, column, and diagonal brace, respectively.



CBF EBF

a) 4 story

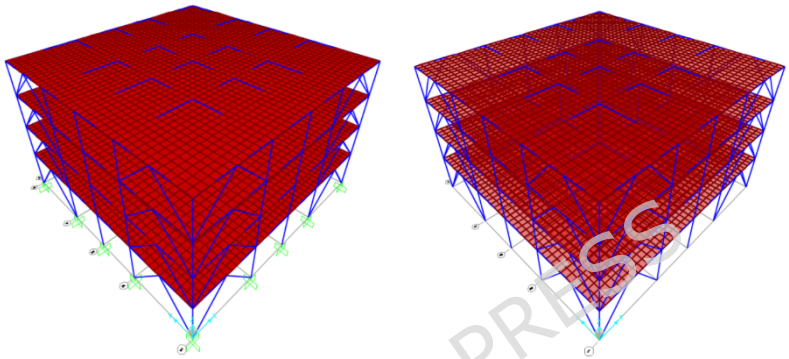
ARTICLE IN PRESS



CBF EBF

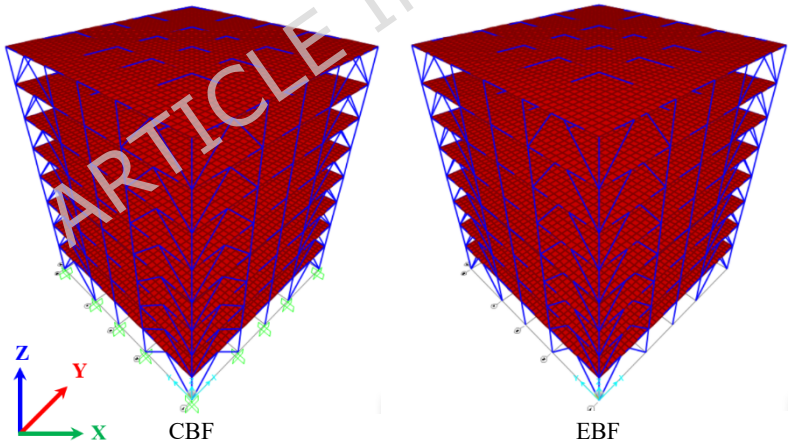
b) 8 story

Figure 6 Two-dimensional view of CBF and EBF (a) 4-story and (b) 8-story building models



CBF EBF

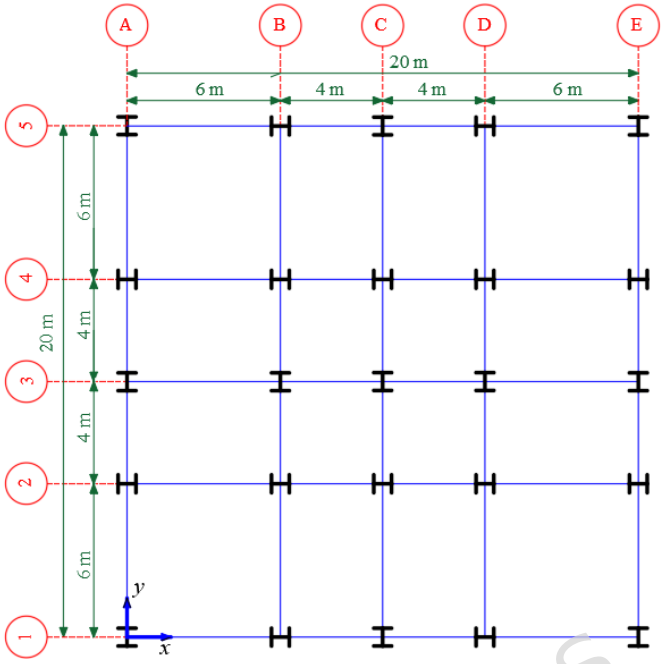
a) 4-story



CBF EBF

b) 8-story

ARTICLE IN PRESS



c) floor plan

Figure 7 3D model of the building for CBF and EBF (a) 4-story, (b) 8-story and (c) floor plan of the model

3. Results and Discussion

3.1. Modal results

This study aims to investigate the dynamic behavior of CBF and EBF systems for 4- and 8-story buildings subjected to NFGEs. NTHAs were carried out to evaluate the dynamic response characteristics of the considered building configurations. A total of 12 NFGEs, classified according to LP, MP, and SP periods, were selected for the analyses. The modal properties obtained from the modal analysis of the CBF and EBF systems are summarized in **Table 4** and the first three mode shapes are illustrated in **Figure 8**. The fundamental mode is dominated by translational motion, while the second mode represents translation in the orthogonal direction, indicating a relatively uniform lateral stiffness distribution. The third mode exhibits significant torsional behavior, highlighting the contribution of three-dimensional effects in the structural response. The modal analysis results indicate noticeable differences in the natural periods and frequencies of the structures depending on both the number of stories and the inverted-V bracing configuration. As expected, the fundamental period increases with increasing building height for both CBF and EBF systems, reflecting the reduction in global stiffness associated with taller structures. For the 4-story buildings, the fundamental period of the CBF system is 0.207 s, whereas it increases to 0.244 s for the EBF system. This corresponds to a reduction of approximately 15.2% in the fundamental period of the CBF configuration compared to the EBF configuration, indicating a stiffer structural response. Similarly, for the 8-story buildings, the fundamental period of the CBF system is 0.437 s, while that of the EBF system is 0.532 s, representing a reduction of about 17.8% in the fundamental period for the CBF system. These results demonstrate that, for both building heights, the CBF configuration exhibits shorter natural periods and higher modal frequencies than the corresponding EBF configuration. This behavior confirms that the CBF system provides higher global stiffness compared to the EBF system. Overall, the observed trend is

ARTICLE IN PRESS

consistent with theoretical expectations, whereby increased building height leads to longer natural periods, while stiffer bracing configurations result in reduced fundamental periods.

Table 4 Modal properties for CBFs and EBFs

Mod	*4-Story*				*8-Story*			
	CBF		EBF		CBF		EBF	
	T (s)	f (Hz)	T (s)	f (Hz)	T (s)	f (Hz)	T (s)	f (Hz)
1	0.20697	4.83165	0.24396	4.09905	0.43702	2.28823	0.53167	1.88085
2	0.20467	4.88588	0.24001	4.16643	0.43386	2.30492	0.52774	1.89488
3	0.14199	7.04233	0.16752	5.96915	0.29140	3.43170	0.36850	2.71368
4	0.09817	10.18680	0.09870	10.13159	0.14507	6.89307	0.17718	5.64409
5	0.09807	10.19722	0.09851	10.15149	0.14367	6.96028	0.17536	5.70255

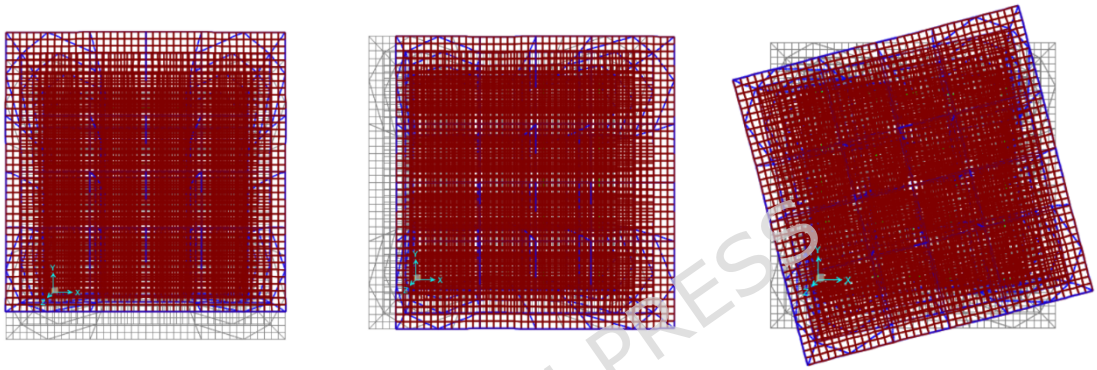


Figure 8 Mode shapes of the building models

3.2. Lateral floor displacement

The displacement performance differences between CBF and EBF for all scenarios and building heights are highlighted in **Table 5**. Maximum story displacements of the CBF and EBF for 4- and 8-story under NFGEs, including SP, MP, and LP scenarios, are depicted in **Figures 9-11**, respectively. In these figures, the solid lines represent the CBF system, whereas the dashed lines correspond to the EBF system.

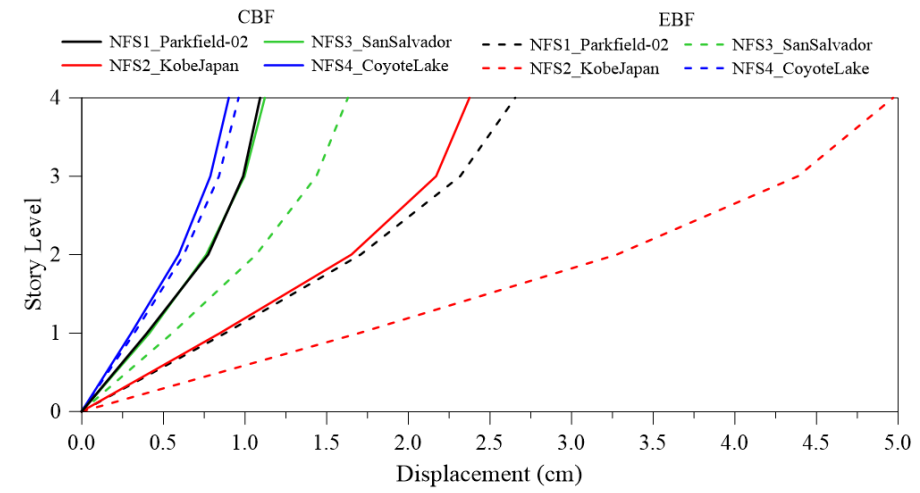
Figure 9 presents the maximum story displacement envelopes along the height of the 4-story CBF and EBF models subjected to the NFS, NFM, and NFL pulse sets. For the selected NFGEs, the displacement demand generally increases with story height, and the maximum values occur at the roof level. Overall, the EBF model develops higher peak story displacements than the CBF model. This behavior is mainly associated with the lower initial lateral stiffness of the EBF system and the intended yielding mechanism of the link elements, whereas the higher initial stiffness of the CBF system limits lateral displacement demand more effectively. Considering the modal properties given in Table 4, the fundamental period of the 4-story model is approximately $T_1 \approx 0.207s$ for the CBF and $T_1 \approx 0.244s$ for the EBF. In contrast, the selected pulse periods listed in **Table 1** range between $T_p \approx 1.08s - 1.16s$ for NFS, $T_p \approx 1.62s - 2.99s$ for NFM, and $T_p \approx 3.53s - 6.19s$ for NFL motions. Therefore, for all pulse groups, (T_p) is considerably larger than (T_1), indicating that the response is not governed by classical resonance, but rather by an off-tuned impulsive response mechanism associated with velocity-pulse momentum and energy transfer. In **Figure 9a** (in the case of NFS pulse), the largest displacement demand for both systems occurs under the NFS2 (Kobe) record. Consistent with the displacement profiles, the top floor displacement reaches

ARTICLE IN PRESS

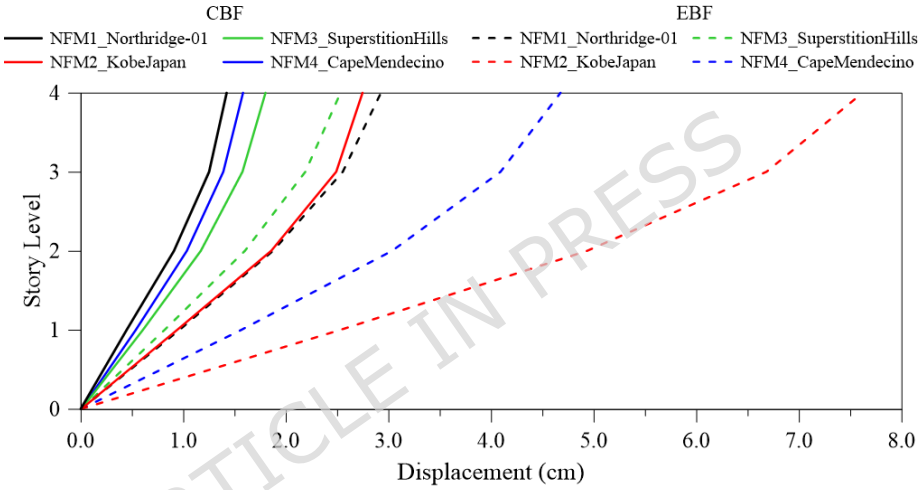
approximately 2.37 cm in the CBF system and about 5.0 cm in the EBF system. The highest PGV (76.11 cm/s) and PGA (0.63g) are observed NFS2 whereas the lowest PGV (29.58 cm/s) and PGA (0.26g) observed NFS4 (Coyote Lake) record (see, **Table 1**). The relatively high PGV and PGA of NFS2 Kobe record, combined with a pulse period ($T_p \approx 1.09s$) much larger than T_1, indicates that a short-duration but high-momentum pulse significantly amplifies the structural response. Conversely, the lowest displacement demand is observed for the NFS4 (Coyote Lake) record having the lowest PGA and PGV, where both systems exhibit similar roof displacements (0.90cm for CBF and 0.96cm for EBF). Consequently, for records with comparable PGV/PGA characteristics, ground motions combining high PGV with moderately lower T_p/T_1 ratios tend to induce the most severe displacement responses, particularly in the more flexible EBF systems in the selected records. This highlights that seismic demand under near-fault pulse excitations is controlled by a combined interaction of pulse timing and velocity amplitude, rather than by T_p/T_1 alone. In **Figure 9b** (in the case of NFM pulse), displacement demands are generally higher than those observed under NFS excitations, and the difference between the two structural systems becomes more pronounced. Similar to the other pulse groups, displacement demand increases monotonically with story height for all records, with peak values occurring at the top level. Among the selected NFM records, NFM2 (Kobe) produces the largest displacement demand in both structural systems. The top floor displacement reaches 2.74 cm in the CBF system and 7.61 cm in the EBF system, consistent with the values reported in **Table 6**. This response can be attributed to the combined effects of relatively high PGV (≈86 cm/s) and large PGA (≈0.6 g), together with a pulse period of $T_p = 1.81s$, which is significantly longer than the fundamental periods of the 4-story frames. For the NFL pulse group shown in **Figure 9c**, the largest displacement demands are observed among all pulse categories. The NFL4 (Tabas, Iran) record produces the maximum roof displacements, reaching approximately 4.15 cm for the CBF and 11.02 cm for the EBF. This record has the longest pulse period and the highest PGV and PGA values among the NFL motions. Therefore, the amplified roof displacement response can be explained by the combined influence of long pulse duration, high velocity amplitude, and cumulative momentum transfer. In contrast, the lowest displacement demand is observed under the NFL3 (Kocaeli, Türkiye) record, which has the lowest PGA and PGV values, despite its relatively large (T_p/T_1) ratio.

Overall, the displacement response of the 4-story models indicates that the CBF system generally limits lateral floor displacements more effectively than the EBF system owing to its higher initial lateral stiffness. However, the larger displacements observed in the EBF model should not be interpreted directly as less favorable structural behavior, since they are associated with the more flexible response mechanism and the intended yielding of link elements for energy dissipation. The results also show that the displacement demand under NFGEs is not governed by pulse period or (T_p/T_1) ratio alone. Instead, the response is controlled by the combined effect of pulse intensity, particularly PGV and PGA, T_p/T_1, and the nonlinear deformation mechanism of the bracing system. For the selected 4-story case-study frames, short- and medium-period pulses with relatively high PGV produced significant displacement demands even when (T_p/T_1) was not the largest, whereas the long-period pulse group produced the highest overall displacement demands due to the combined influence of large PGV, long pulse duration, and cumulative momentum transfer. Therefore, Figure 9 should be interpreted as evidence of record-dependent response trends for the selected models, rather than as a general conclusion on the superiority of one bracing system or the isolated effect of pulse duration.

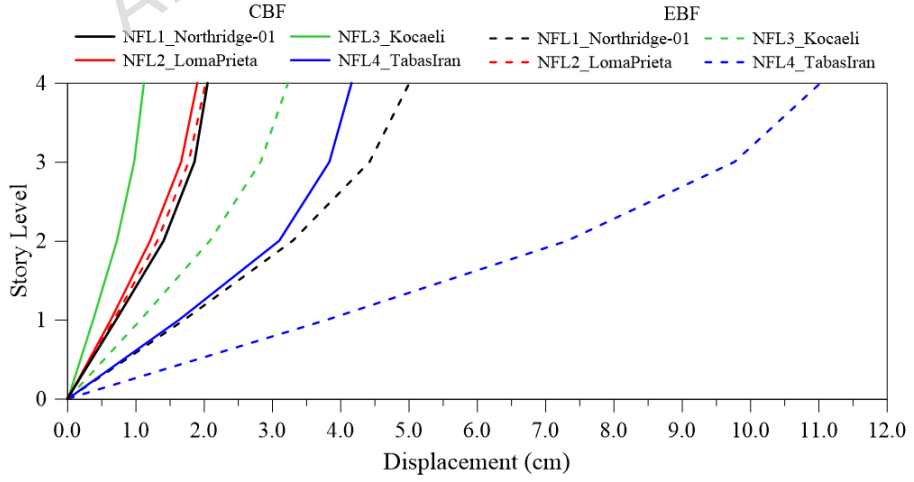
ARTICLE IN PRESS



a) NFS pulse



b) NFM pulse



c) NFL pulse

Figure 9 Comparison of maximum displacement a) NFS, b) NFM and c) NFL pulse effect on 4-story system

ARTICLE IN PRESS

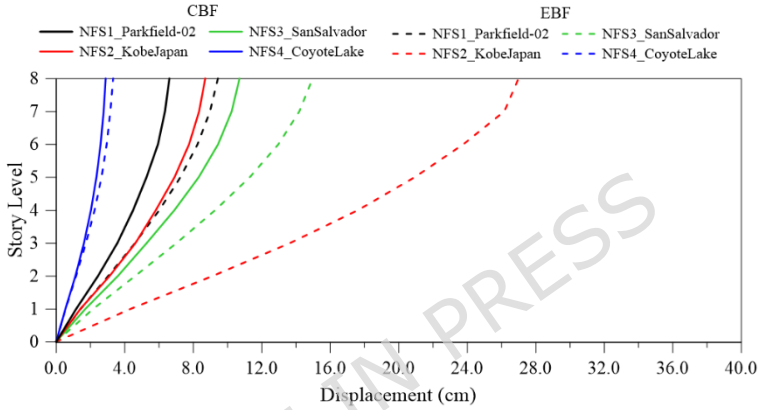
Figure 10 presents the maximum story displacement envelopes of the 8-story CBF and EBF models under the NFS, NFM, and NFL pulse sets. The displacement demands generally increase with elevation and reach their maximum values at the roof level. Unlike the 4-story models, where the NFL records produced the largest displacements, the 8-story models exhibit their peak displacement demands mainly under the NFM records. This shift can be explained by the change in dynamic compatibility between the pulse period and the structural period as the building height increases. In the 4-story models, T_1 is much shorter than the NFL pulse periods, so the response is mainly governed by impulsive momentum input from long-period, high-PGV records. In the 8-story models, the longer fundamental periods reduce the T_p/T_1 ratios and bring the response closer to the effective range of medium-period pulses. Therefore, NFM records can transfer pulse-induced momentum more efficiently into the dominant deformation mode of the taller frames, resulting in larger displacement demands than NFL records for the selected 8-story models. For the NFS pulse group shown in **Figure 10a** and **Table 6**, the largest top-floor displacement occurs under the NFS3 record for the CBF system and under the NFS2 record for the EBF system. Although the pulse periods of the NFS records are close to each other, their displacement demands differ noticeably. This indicates that, within the narrow (T_p/T_1) range of the NFS set, the response is influenced mainly by pulse intensity measures, particularly PGV and PGA, together with the stiffness characteristics of the structural system. The EBF system is more sensitive to high-intensity velocity pulses because of its lower initial stiffness and link-yielding mechanism, whereas the CBF response appears more affected by record-specific pulse characteristics and the distribution of deformation along the height. For the NFM pulse group shown in **Figure 10b**, both systems experience their maximum displacement demands under the NFM2 record and their minimum demands under the NFM1 record. Although the (T_p/T_1) ratios of NFM2 are not the largest within the group, this record has considerably higher PGV and PGA values than NFM1. Therefore, the larger response under NFM2 can be explained by the combined influence of pulse intensity, effective momentum transfer, and pulse timing relative to the structural period. The much larger displacement demand in the EBF model reflects its more flexible lateral response and distributed link-yielding mechanism, which allows high-intensity velocity pulses to produce larger global deformation. For the NFL pulse group shown in **Figure 10c**, the largest displacement demand occurs under the NFL4 record in both systems. This record combines the longest pulse period with the highest PGV and PGA values within the NFL set, leading to significant accumulation of lateral displacement toward the upper stories. However, the NFL demands are generally lower than those induced by the NFM set in the 8-story models. This suggests that the response of the taller frames is not governed by long pulse duration alone. Instead, the closer interaction between the structural period and the medium-period pulses may produce more efficient momentum transfer and larger displacement amplification.

Overall, the displacement response of the 8-story models indicates that the governing pulse group changes with building height because the longer structural periods reduce the (T_p/T_1) ratios and alter the interaction between pulse timing and structural deformation modes. The CBF system generally limits lateral displacements more effectively because of its higher initial stiffness, whereas the EBF system develops larger roof displacements due to its more flexible configuration and link-yielding mechanism. The results also show that displacement demand is not controlled by (T_p/T_1), PGV, PGA, or pulse duration individually, but by their combined interaction with the nonlinear response mechanism of the bracing system.

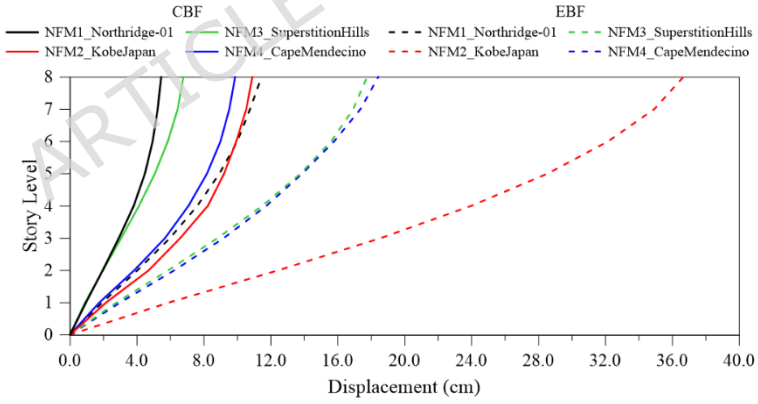
Table 5 Pulse period to structure period ratio (T_p/T_1) for the selected NFGEs in 4- and 8-story systems

ARTICLE IN PRESS

Excitation Type		*Earthquake*	T_P *(s)*	$\frac{T_P}{T_1}$			
				4-story		8-story	
				CBF	*EBF*	*CBF*	*EBF*
*NFS**	NFS1	Parkfield-02, CA	1.08	5.22	4.43	2.47	2.08
	NFS2	Kobe, Japan	1.09	5.27	4.48	2.49	2.05
	NFS3	San Salvador	1.13	5.48	4.63	2.58	2.13
	NFS4	Coyote Lake	1.16	5.60	4.75	2.65	2.18
*NFM**	NFM1	Northridge-01	1.62	7.83	6.64	3.71	3.05
	NFM2	Kobe, Japan	1.81	8.74	7.42	4.14	3.40
	NFM3	Superstition Hills-02	2.39	11.55	9.79	5.47	4.49
	NFM4	Cape Mendocino	2.99	14.45	12.26	6.84	5.62
*NFL**	NFL1	Northridge-01	3.53	17.06	14.46	8.08	6.64
	NFL2	Loma Prieta	4.57	22.08	18.73	10.46	8.60
	NFL3	Kocaeli, Turkey	5.37	25.94	22.01	12.29	10.10
	NFL4	Tabas, Iran	6.19	29.91	25.37	14.16	11.83



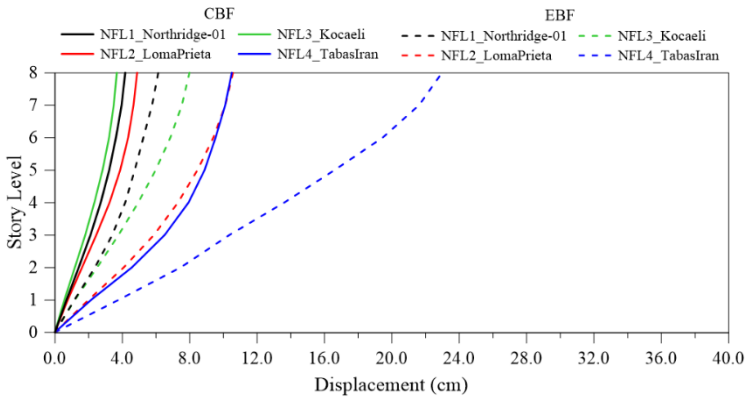
a) NFS pulse



b) NFM pulse

ARTICLE IN PRESS

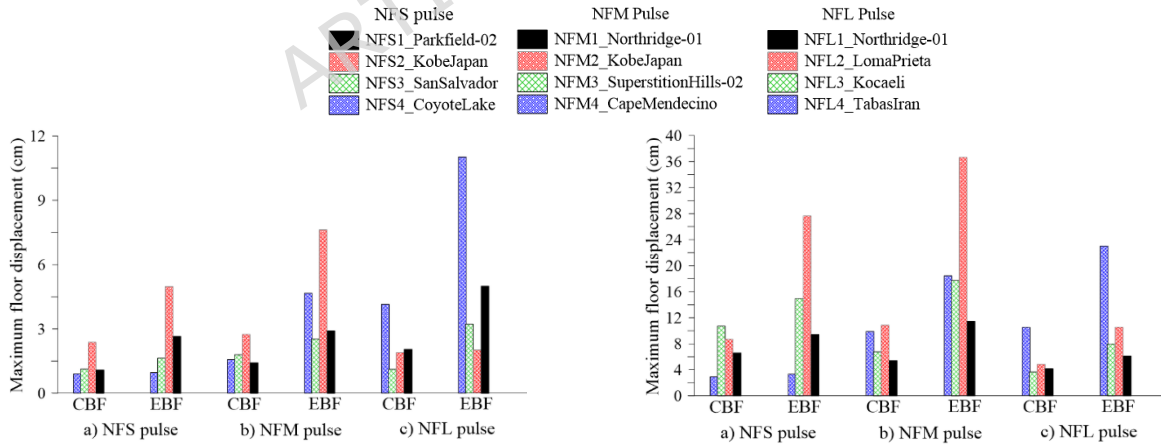
ARTICLE IN PRESS



c) NFL pulse

Figure 10 Comparison of maximum displacement a) NFS, b) NFM and c) NFL pulse effect on 8-story system

Figure 11 compares the displacement differences between the CBF and EBF systems for the 4- and 8-story frames under the selected NFGEs. The EBF systems generally develop larger top-floor displacements than the corresponding CBF systems, and this difference becomes more pronounced in the 8-story frames. This trend is mainly related to the lower initial lateral stiffness of the EBF configuration and the intended yielding of the link elements, which allow larger but more uniformly distributed global deformations. In contrast, the higher initial stiffness of the CBF system limits lateral displacement demands more effectively, although brace yielding or buckling may result in more localized deformation patterns. The change in the governing pulse group from NFL in the 4-story models to NFM in the 8-story models indicates that displacement demand is governed by the combined interaction of structural period, pulse timing, pulse intensity, and nonlinear deformation mechanism rather than by pulse duration alone. Therefore, the results should be interpreted as record-dependent response trends for the selected models, not as a general conclusion on the superiority of one bracing system.



i) 4-story ii) 8-story

Figure 11 Max floor displacement comparison for CBF and EBF i) 4-story and ii) 8-story system

Table 6 Comparison of top-floor displacement between CBF and EBF models

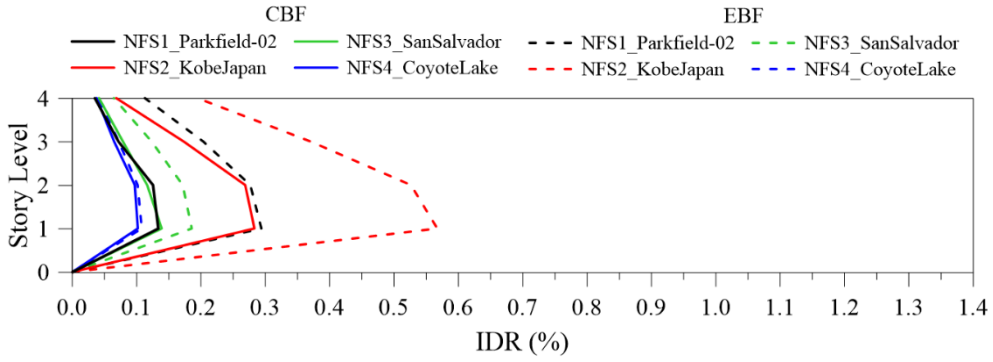
Group	Records	Top-floor displacement (cm)				Variation (%)	
		4-story		8-story			
		CBF	EBF	CBF	EBF	4-story	8-story

ARTICLE IN PRESS

NFS	NFS1_Parkfield-02	1.09	2.65	6.61	9.44	143.12	42.81
	NFS2_KobeJapan	2.37	4.97	8.71	27.69	109.70	217.91
	NFS3_SanSalvador	1.12	1.63	10.71	14.97	45.54	39.78
	NFS4_CoyoteLake	0.90	0.96	2.89	3.32	6.67	14.88
NFM	NFM1_Northridge-01	1.42	2.92	5.44	11.44	105.63	110.29
	NFM2_KobeJapan	2.74	7.61	10.89	36.67	177.74	236.73
	NFM3_SuperstitionHills-02	1.79	2.52	6.77	17.75	40.78	162.19
	NFM4_CapeMendecino	1.57	4.67	9.87	18.42	197.45	86.63
NFL	NFL1_Northridge-01	2.05	4.99	4.17	6.13	143.41	47.00
	NFL2_LomaPrieta	1.89	2.01	4.88	10.57	6.35	116.60
	NFL3_Kocaeli	1.11	3.22	3.67	7.99	190.09	117.71
	NFL4_TabasIran	4.15	11.02	10.51	22.99	165.54	118.74

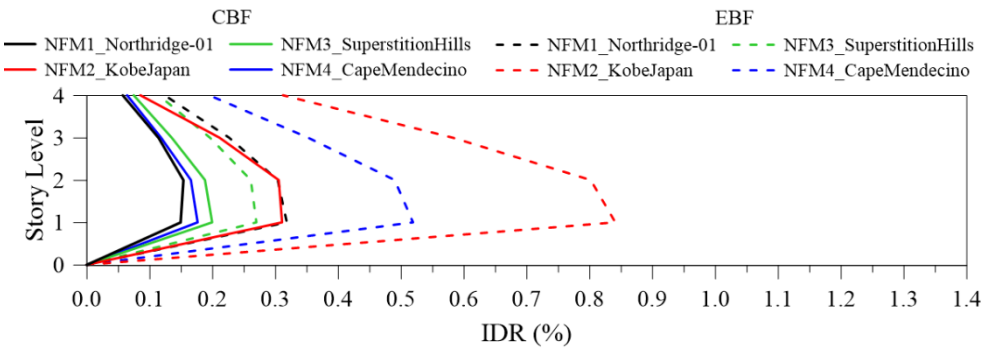
3.3. Inter-story drift ratio (IDR)

Figure 12 presents the IDR distributions of the 4-story CBF and EBF systems under selected NFS, NFM, and NFL pulse-type ground motions. For all pulse categories, the maximum drift demands are consistently observed in the EBF system, reflecting its lower effective lateral stiffness and higher deformation capacity compared to the CBF system. Under NFS motions, the NFS2 (Kobe) record governs the drift response, producing a peak IDR of approximately 0.55% in the EBF model, while the remaining NFS records induce relatively low and closely clustered drifts, particularly in the CBF system. The larger separation among EBF responses suggests a greater record-to-record variability under short-duration velocity pulses, which may be associated with pulse intensity effects (PGV/PGA) in flexible systems. In **Figure 12a,** for NFS records, the EBF system exhibits a wider spread in IDR responses across different motions compared to the CBF system, indicating a more pronounced record-to-record variability. In **Figure 12b** for the NFM set, NFM2 (Kobe) again controls the maximum drift demand, with peak IDR values approaching 0.85% in the EBF system. In contrast, NFM1, NFM3, and NFM4 exhibit similar and lower drift levels in the CBF model, highlighting the dominant role of pulse intensity (PGV/PGA) in governing drift demand for medium-pulse motions. In **Figure 12c** Under NFL excitations, the largest drift demands occur for the NFL4 (Tabas) record, reaching approximately 1.25% in the EBF system. The long-duration velocity pulse leads to pronounced drift amplification along the height, indicating a momentum-dominated response mechanism in the short-period 4-story structure. Overall, the results demonstrate that for 4-story buildings, drift demand is primarily controlled by pulse intensity and duration, while the EBF system consistently exhibits larger drifts than the CBF system due to its higher flexibility and distributed inelastic response.

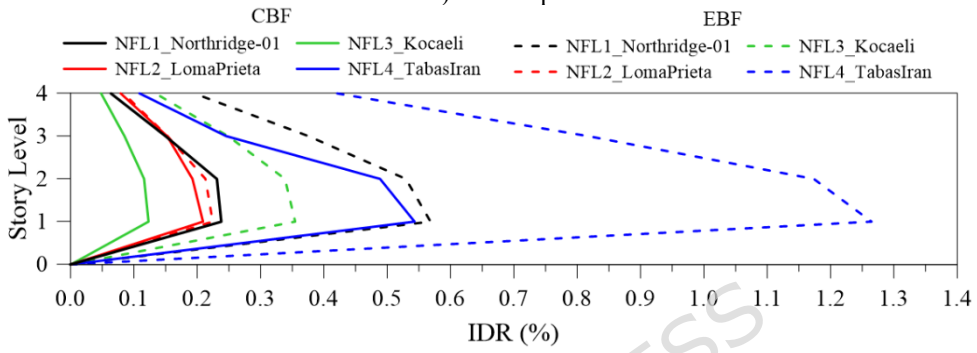


a) NFS pulse

ARTICLE IN PRESS



b) NFM pulse



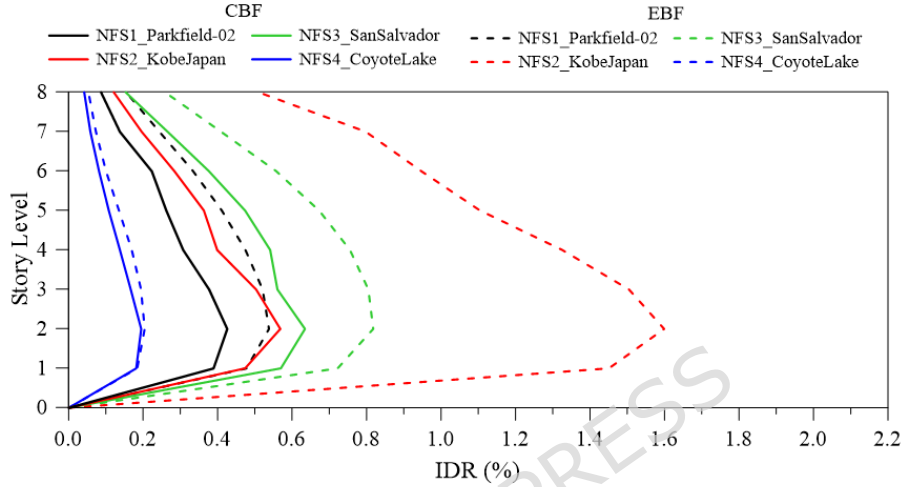
c) NFL pulse

Figure 12 Comparison of IDRs between CBF and EBF models for 4-story building

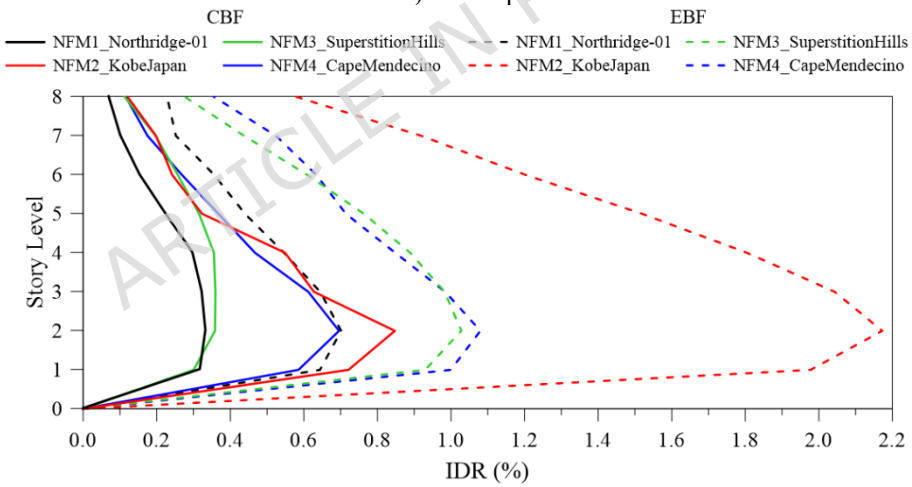
Figure 13 compares the IDR distributions of the 8-story CBF and EBF systems under the selected NFS, NFM, and NFL pulse motions. Compared with the 4-story configuration, the 8-story models exhibit a more pronounced concentration of drift demands in the lower stories, particularly around the first and second floors. For the NFS pulse group shown in **Figure 13a**, the maximum IDR occurs under the NFS3 record in the CBF system and under the NFS2 record in the EBF system. Since the NFS records have similar pulse periods, the differences in IDR demand are mainly related to pulse intensity measures, particularly PGV and PGA, and to record-specific velocity-pulse characteristics. The EBF system develops larger and more distributed drift demands because of its lower effective lateral stiffness and link-yielding mechanism, whereas the CBF system tends to concentrate drift more locally in the lower stories. For the NFM pulse group shown in **Figure 13b**, both systems reach their maximum IDR demands under the NFM2 record, with peak drifts concentrated near the second story. Although this record does not have the largest T_p/T_1 ratio within the NFM set, its high velocity-pulse intensity produces a more effective momentum transfer to the 8-story frames. This explains why the largest overall IDR demand is observed under NFM2, especially in the EBF system. Therefore, the NFM results indicate that medium-period pulses can be particularly critical for the 8-story models when their intensity and timing interact efficiently with the structural period and deformation mechanism. For the NFL pulse group shown in **Figure 13c**, the largest IDR demands are produced by the NFL4 record in both systems. This response is associated with the combined effect of long pulse duration, high velocity amplitude, and large momentum input. However, the NFL results also show that large (T_p/T_1) ratios alone do not necessarily lead to the largest drift demand, since records with lower PGV and PGA values produce considerably smaller IDRs despite having large period ratios. Thus, for long-period pulses, (T_p/T_1) acts more as an amplifying condition when accompanied by high pulse intensity, rather than as the sole governing parameter.

ARTICLE IN PRESS

Overall, the IDR response of the 8-story frames indicates that drift demand is controlled by the combined interaction of pulse intensity, pulse timing, structural period, and the nonlinear deformation mechanism of the bracing system. The EBF system consistently develops larger IDR demands because its lower lateral stiffness and link-yielding mechanism allows greater global deformation, while the CBF system limits overall drift more effectively but may concentrate deformation in lower stories after brace yielding or buckling. Therefore, **Figure 13** should be interpreted as presenting record-dependent IDR trends for the selected 8-story models, rather than as a general conclusion regarding the isolated influence of pulse characteristics or the overall superiority of one bracing system.

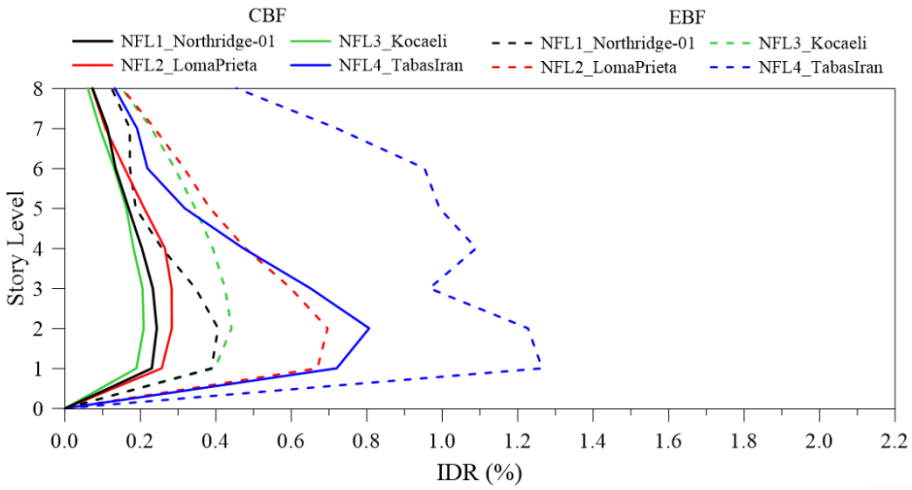


a) NFS pulse



b) NFM pulse

ARTICLE IN PRESS



c) NFL pulse

Figure 13 Comparison of IDRs between CBF and EBF models for 8-story buildings

A combined evaluation of **Figures 10-11** and **Figures 12-13** indicates that near-fault pulse characteristics influence structural response through an interaction between global displacement demand and inter-story drift distribution. Records with high velocity-pulse intensity and effective momentum input tend to amplify global displacement demands, which are then transformed into IDR demands depending on the lateral stiffness and nonlinear deformation mechanism of the structural system. The EBF systems generally develop larger global displacements because of their lower effective lateral stiffness; however, their link-yielding mechanism allows these deformations to be distributed more uniformly along the height. In contrast, the CBF systems generally limit global displacements more effectively, but drift demands may become more localized in fewer stories after brace yielding or buckling. Therefore, the observed displacement and IDR responses should be interpreted as record-dependent trends governed by the combined effects of pulse intensity, pulse timing, structural period, and bracing-system deformation mechanism.

Table 7 presents a comparison of the maximum IDR demands obtained from the 4- and 8-story CBF and EBF models. The results show that the EBF system consistently produces larger maximum IDR demands than the corresponding CBF system for all selected pulse records and both building heights. For the 4-story models, the EBF/CBF IDR ratio ranges from 1.10 to 2.92, corresponding to an increase of approximately 10% to 191%. For the 8-story models, this ratio ranges from 1.05 to 2.91, with the IDR increase varying between approximately 5% and 191%. Among the pulse groups, the largest relative differences are generally observed under NFM and NFL records. In the 4-story models, the highest EBF/CBF ratio is obtained under NFL3, whereas in the 8-story models, the largest ratio occurs under NFM3. This indicates that the relative drift amplification in EBF systems is not governed by pulse category alone, but by the combined effects of pulse intensity, structural period, and bracing-system deformation mechanism. Overall, this comparison confirms that the CBF system limits maximum IDR demands more effectively due to its higher initial lateral stiffness. In contrast, the EBF system develops larger drift demands because of its lower effective stiffness and link-yielding mechanism. Therefore, the table clearly illustrates the stiffness–ductility trade-off between the two systems and provides a direct quantitative basis for comparing their seismic response under the selected NFGEs.

Table 7 Comparison of max IDR results between CBF and EBF models

Group	Records	Max IDR (%)

ARTICLE IN PRESS

		4-story				8-story			
		CBF	EBF	EBF/CBF ratio	Variation (%)	CBF	EBF	EBF/CBF ratio	Variation (%)
NFS	NFS1	0.13	0.29	2.23	123	0.42	0.53	1.26	26
	NFS2	0.28	0.57	2.04	103	0.56	1.59	2.84	183
	NFS3	0.13	0.18	1.38	38	0.63	0.81	1.29	28
	NFS4	0.10	0.11	1.10	10	0.19	0.20	1.05	5
NFM	NFM1	0.15	0.32	2.13	113	0.33	0.70	2.12	112
	NFM2	0.31	0.84	2.71	170	0.84	2.17	2.58	158
	NFM3	0.20	0.27	1.35	35	0.35	1.02	2.91	191
	NFM4	0.18	0.52	2.89	188	0.69	1.08	1.57	56
NFL	NFL1	0.23	0.56	2.43	143	0.24	0.41	1.71	71
	NFL2	0.20	0.22	1.10	10	0.28	0.69	2.46	146
	NFL3	0.12	0.35	2.92	191	0.21	0.44	2.10	109
	NFL4	0.54	1.27	2.35	135	0.80	1.26	1.58	57

Table 8 summarizes the mean and COV values of the maximum IDR demands for the 4- and 8-story CBF and EBF models. The results show that the EBF systems consistently produce higher mean IDR demands than the corresponding CBF systems for all pulse groups and both building heights. For the 4-story models, the highest mean IDR values are obtained under the NFL pulse group, whereas for the 8-story models, the highest mean IDR values occur under the NFM pulse group. This confirms that the governing pulse group changes with building height and structural period. The COV values range from approximately 33% to 77%, indicating noticeable record-to-record variability within the selected pulse groups. Therefore, the statistical results support the main response trends observed in the deterministic comparisons, while also showing that the findings should be interpreted as record-dependent rather than statistically generalized conclusions.

Table 8 Statistical summary of maximum IDR demands for CBF and EBF models

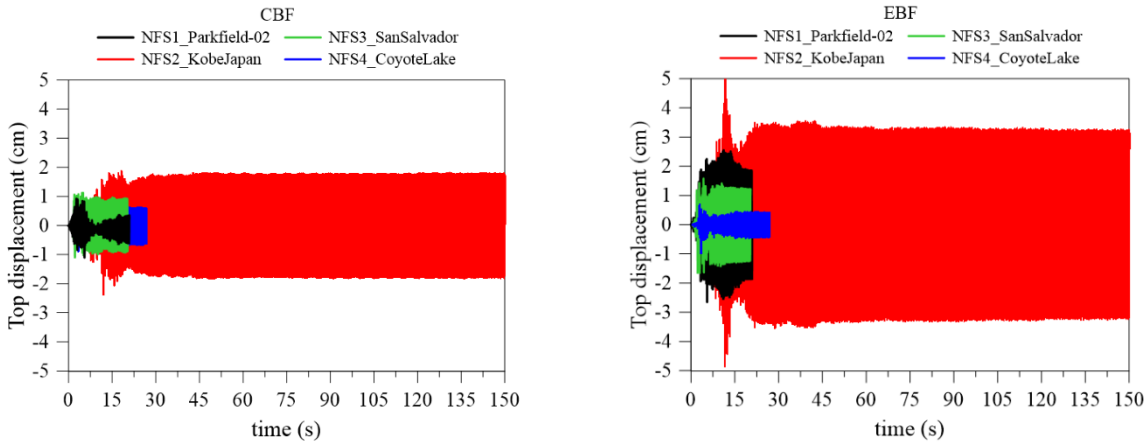
Structural model	Records	Max IDR (%) values	Mean IDR (%)	SD	COV (%)
4-story CBF	NFS1 -NFS4	0.13 – 0.28 – 0.14 – 0.10	0.164	0.081	49.27
	NFM1-NFM4	0.15 – 0.31 – 0.20 – 0.17	0.210	0.070	33.16
	NFL1 -NLF4	0.24 – 0.21 – 0.12 – 0.54	0.278	0.183	65.83
4-story EBF	NFS1 -NFS4	0.29 – 0.57 – 0.18 – 0.11	0.288	0.201	69.61
	NFM1-NFM4	0.32 – 0.84 – 0.27 – 0.52	0.487	0.259	53.26
	NFL1 -NLF4	0.57 – 0.22 – 0.35 – 1.26	0.602	0.463	76.91
8-story CBF	NFS1 -NFS4	0.43 – 0.57 – 0.63 – 0.19	0.455	0.195	42.77
	NFM1-NFM4	0.33 – 0.85 – 0.36 – 0.70	0.559	0.254	45.38
	NFL1 -NLF4	0.24 – 0.28 – 0.21 – 0.81	0.385	0.282	73.41
8-story EBF	NFS1 -NFS4	0.54 – 1.60 – 0.82 – 0.20	0.789	0.595	75.42
	NFM1-NFM4	0.70 – 2.17 – 1.03 – 1.08	1.246	0.640	51.40
	NFL1 -NLF4	0.40 – 0.69 – 0.44 – 1.26	0.701	0.397	56.59

3.4. Top displacements

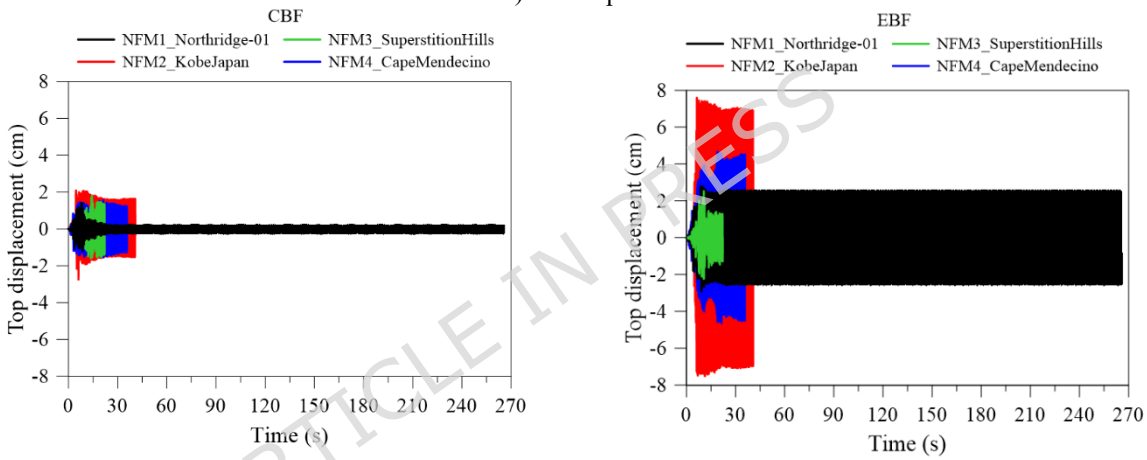
Figures 14-15 present the top-floor displacement time-history responses of the 4- and 8-story CBF and EBF systems under the selected NFGEs. These histories show that the velocity pulse does not necessarily coincide with the instant of maximum roof displacement. Instead, the pulse acts as an impulsive input that transfers momentum to the structure and initiates a subsequent oscillatory response, whose amplitude and decay depend on the structural period, effective stiffness, and nonlinear deformation mechanism. For the 4-story models, the response remains relatively short in duration under NFS records but becomes larger and more sustained under NFM and NFL records as the pulse duration and velocity amplitude increase (see, **Figure 14**). For the 8-story models, the longer fundamental periods allow a stronger interaction between pulse timing and structural deformation, resulting in more pronounced displacement oscillations, especially

ARTICLE IN PRESS

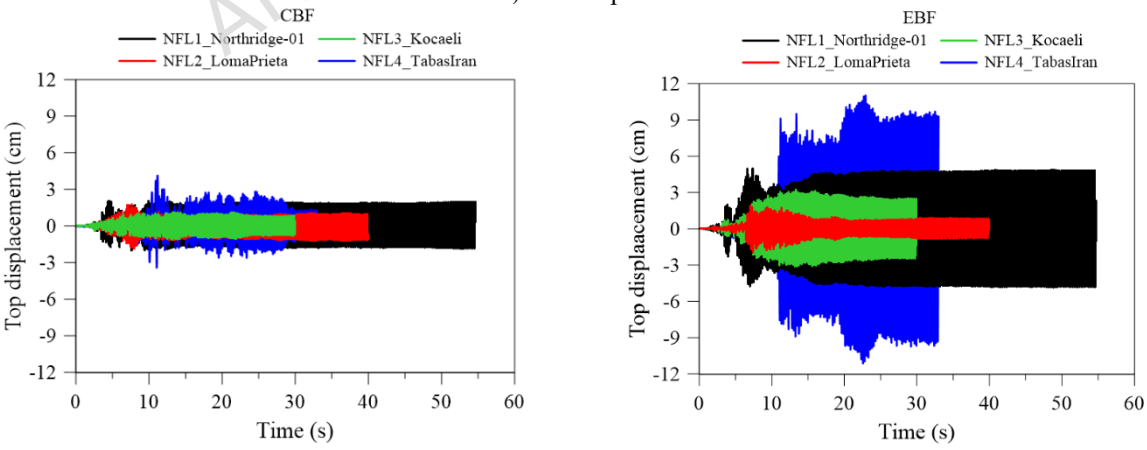
in the EBF system (see, **Figure 15**). The EBF models develop larger amplitudes and slower decay because of their lower effective lateral stiffness and link-yielding mechanism, whereas the CBF models generally limit global displacement more effectively through higher initial stiffness.



a) NFS pulse



b) NFM pulse



c) NFL pulse

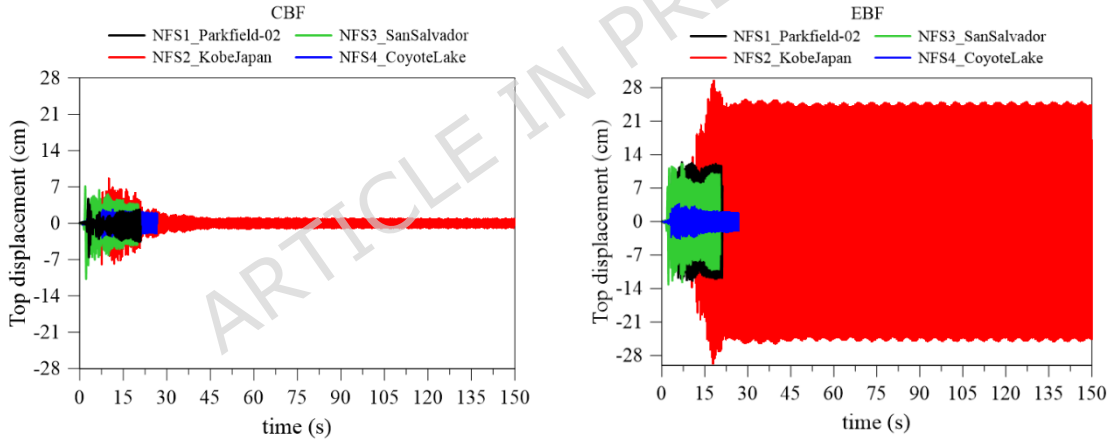
Figure 14 Comparison of top displacements between CBF and EBF models for 4-story buildings

From **Figure 15**, under the NFS records, both systems exhibit relatively limited displacement amplitudes and short effective response durations. Although the EBF system generally develops larger displacements

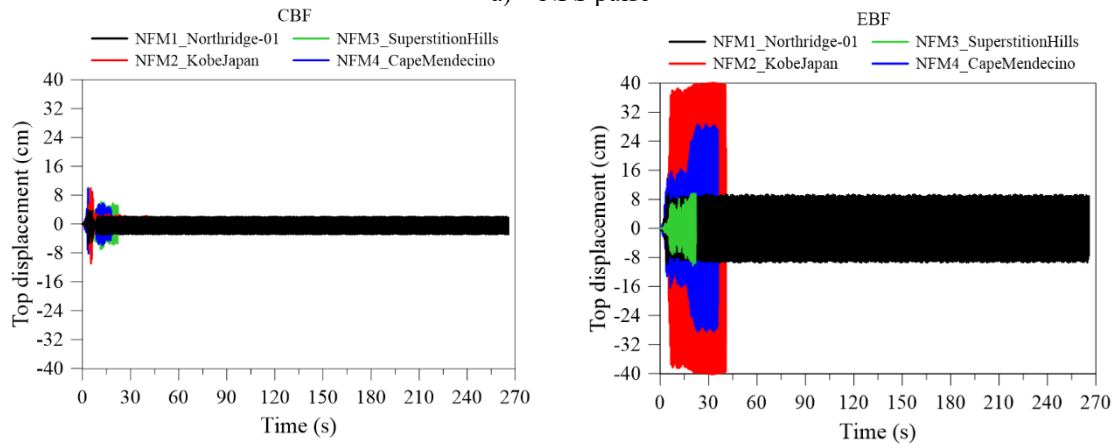
ARTICLE IN PRESS

than the CBF system, the difference between the two systems remains relatively limited under the NFS records. Under the NFM records, the displacement response becomes larger and more persistent, particularly in the EBF system. This can be attributed to the more efficient interaction between medium-period velocity pulses and the longer fundamental periods of the 8-story frames. The lower effective stiffness and link-yielding mechanism of the EBF system allows the pulse-induced momentum input to be transformed into larger global displacement amplitudes, whereas the higher initial stiffness of the CBF system limits the overall displacement response more effectively. Under the NFL records, the response histories exhibit longer-duration oscillations and slower decay, especially in the EBF system. In these cases, the long pulse duration and high velocity amplitude provide a more sustained momentum input, causing the roof displacement response to continue after the main pulse interval. However, the results should not be interpreted as an effect of pulse duration alone, since the observed amplitudes also depend on pulse intensity, timing relative to the structural period, and the nonlinear response mechanism of the bracing system.

Overall, **Figure 15** indicates that the time-history response of the 8-story models is governed by the coupled effects of pulse intensity, pulse timing, structural period, stiffness degradation, and bracing-system deformation mechanism. The EBF system exhibits larger and more sustained roof displacement histories due to its flexible link-yielding response, whereas the CBF system generally limits global displacement but may experience more abrupt response changes when brace yielding or buckling occurs. Therefore, the observed time-history responses should be interpreted as record-dependent dynamic response trends for the selected models rather than as a general conclusion based solely on pulse category.

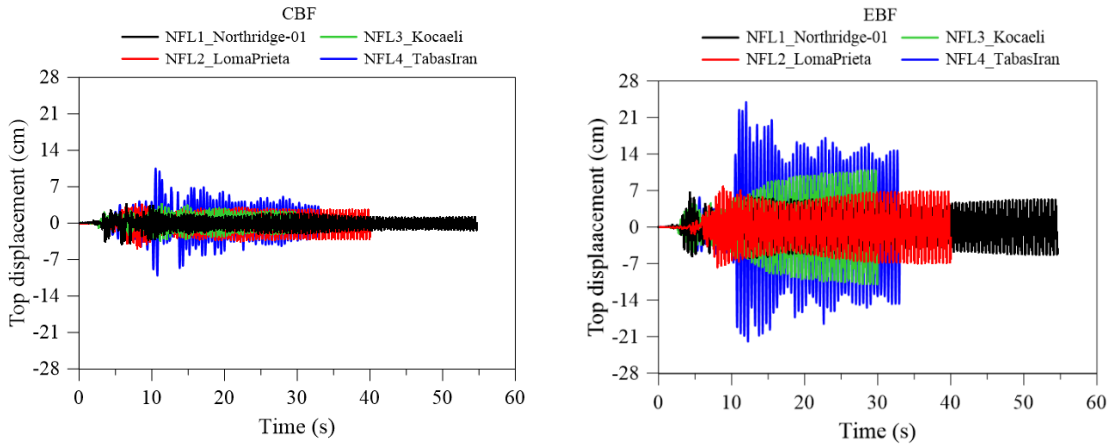


a) NFS pulse



b) NFM pulse

ARTICLE IN PRESS

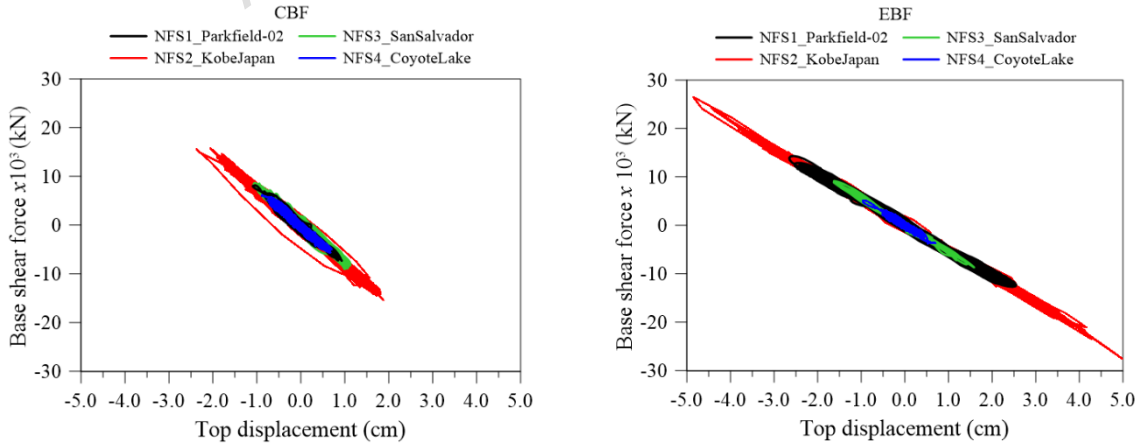


c) NFL pulse

Figure 15 Comparison of top displacements between CBF and EBF models for 8-story buildings under pulse type motions

3.5. Relationship between Base Shear Force and Top Displacement

Figures 16-17 show the base shear force–top-floor displacement relationships of the 4-story and 8-story CBF and EBF systems under the selected NFGEs. The CBF systems generally exhibit steeper response branches, indicating higher initial lateral stiffness and greater base shear mobilization at smaller displacement levels as can be seen in **Figure 16**. In contrast, the EBF systems develop flatter and wider response loops due to their lower effective stiffness and link-yielding mechanism, which allows larger global deformation and more distributed energy dissipation. Under NFS records, the curves remain relatively compact, suggesting limited sustained momentum input from short-duration pulses. Under NFM and NFL records, the curves expand more markedly, especially in the EBF systems, indicating that medium- and long-period pulses are more effective in transferring momentum into nonlinear displacement demand. Therefore, these curves should be interpreted as reflecting the interaction between pulse-induced inertia forces, system stiffness, and nonlinear energy dissipation mechanisms rather than as simple peak force–displacement comparisons.



a) NFS pulse

ARTICLE IN PRESS

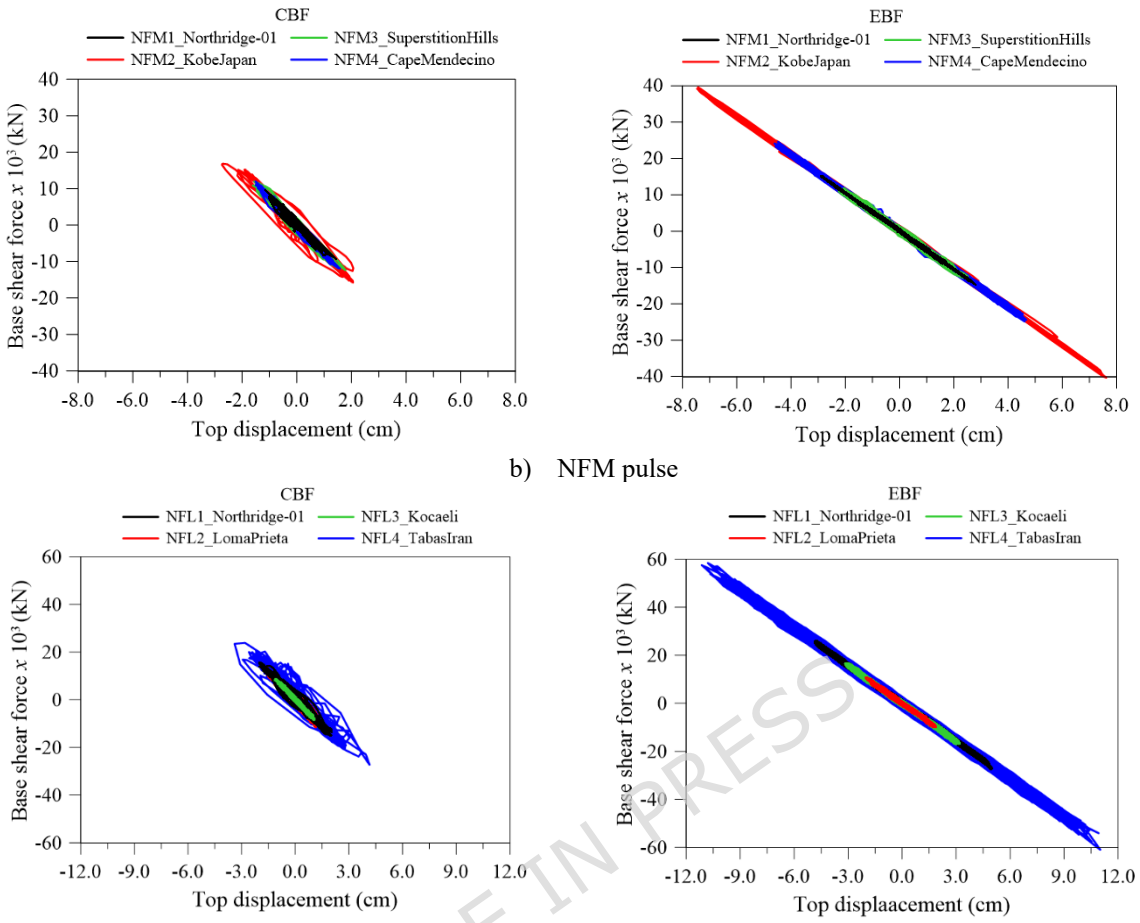
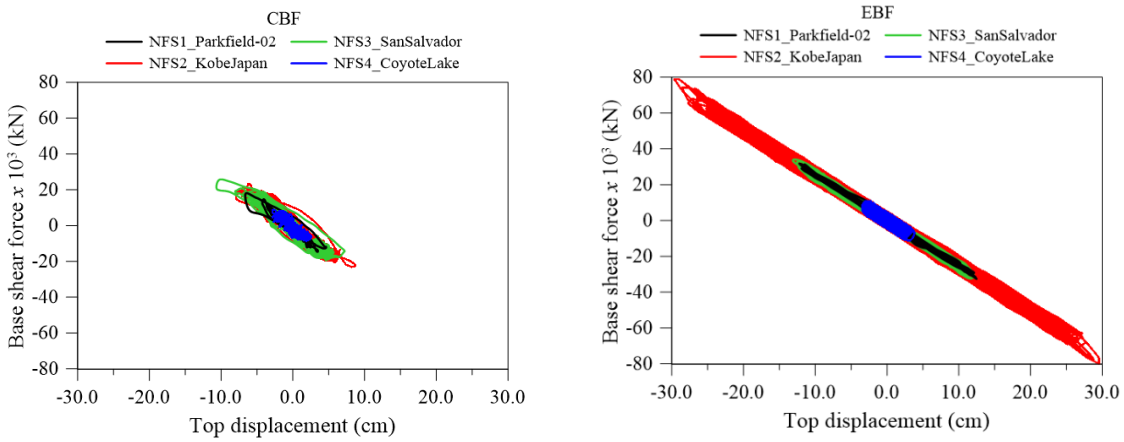


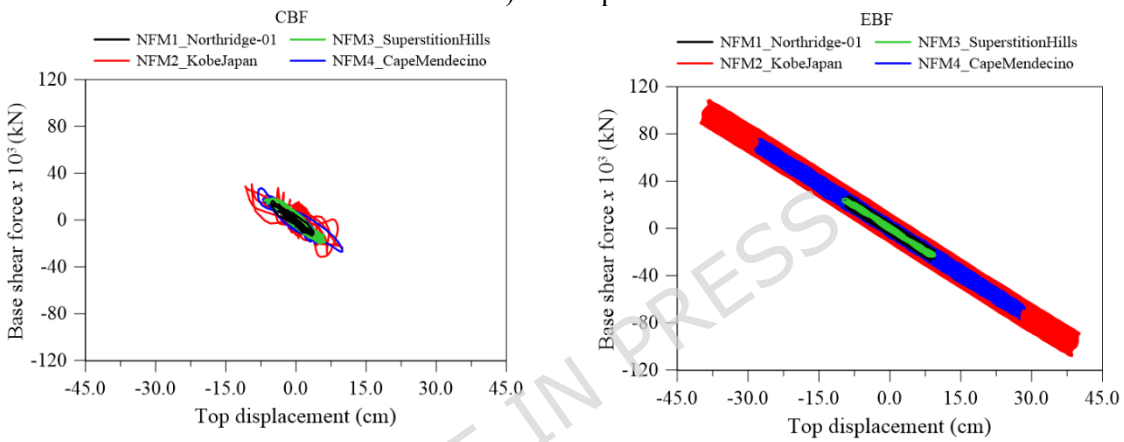
Figure 16 Comparison of base shear forces verse top displacements between CBF and EBF models for 4-story buildings under pulse type motions

As shown in **Figure 17**, in the CBF system, higher base shear forces are mobilized at small displacements, while the EBF system exhibits flatter initial trends. However, under short-period pulse excitation, the overall spread of the curves remains limited in the 8-story systems as well, and differences between the two systems are relatively modest. Under NFM records, the base shear–top floor displacement diagrams of the 8-story systems show a pronounced widening. In particular, the EBF system reaches higher base shear force levels in conjunction with larger displacement demands, resulting in a more distributed response pattern. In contrast, the curves of the CBF system generally cluster within a more compact band. This behavior indicates that, with increasing building height, the responses of EBF and CBF systems become more distinctly separated under medium-period pulses. Under NFL records, the base shear–top floor displacement relationships of the 8-story CBF and EBF systems display the broadest spread. In the EBF system, the curves extend toward substantially larger displacement demands, and under certain records, the base shear forces also reach relatively high levels. In contrast, the curves of the CBF system remain confined to a more limited displacement range.

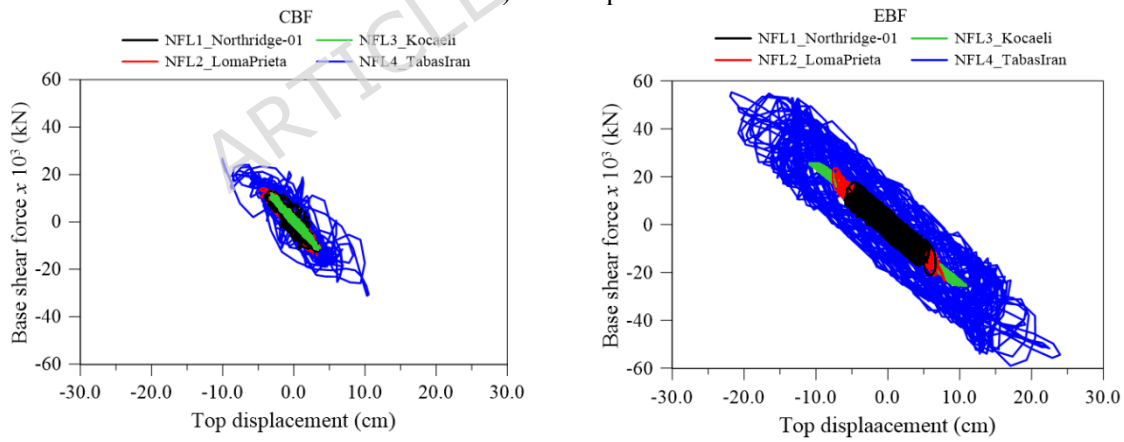
ARTICLE IN PRESS



a) NFS pulse



b) NFM pulse



c) NFL pulse

Figure 17 Comparison of base shear forces verse top displacements between CBF and EBF models for 8-story buildings under pulse type motions

3.6. Story-level distribution of brace performance states under pulse-type earthquakes

Brace performance levels were classified based on hinge state results obtained from NTHAs. The hinge state (A–B–C–D–E) directly reflects the progression of inelastic deformation and was therefore preferred over hinge status, which is dependent on target performance settings and may lead to ambiguous

ARTICLE IN PRESS

interpretation in envelope results. In the analyses, seismic excitations were applied in the global X direction. At each story level, the structural response was evaluated by considering a total of 16 brace members, consisting of 8 braces oriented in the X direction and 8 braces oriented in the Y direction. Accordingly, the 4-story model includes a total of 64 brace elements (16 braces per story), while the 8-story model comprises 128 brace elements in total. This multi-brace configuration ensures that the reported deformation-related performance indices, including IDRs and top-floor displacements, reflect the collective response of a distributed bracing system rather than the behavior of brace members.

Table 8 presents the distribution of brace performance levels along the height of the 4- and 8-story CBF models under the selected pulse records. The results indicate that brace demands become more severe and more vertically distributed as both pulse intensity and building height increase. Under NFS records, the 4-story CBF model remains mostly within the Elastic or IO performance ranges, whereas the 8-story model shows more frequent LS and local CP demands, mainly in the lower stories. This suggests that even short-period pulses may trigger localized brace inelasticity when the structural height increases. Under NFM and NFL records, the brace response shifts from a mostly stiffness-dominated behavior toward a more localized nonlinear mechanism. Inelastic demands initiate in the lower stories and, particularly in the 8-story model, may propagate toward the middle and upper stories. This upward spread reflects the combined effect of stronger velocity-pulse intensity, increased momentum transfer, and reduced elastic response margin in taller frames. However, the damage distribution remains record-dependent, since records with lower PGV and PGA values produce less severe brace demands despite having relatively large pulse-to-structure period ratios. Overall, **Table 8** shows that the high initial stiffness of CBF systems is effective in limiting global displacement, but it may also promote localized brace yielding or buckling when pulse-induced inertia demands exceed the elastic range. Therefore, the observed brace performance levels should be interpreted as record-dependent trends for the selected CBF models rather than as a general damage classification for all near-fault pulse motions.

Table 9 Distribution of brace performance levels per story under different pulse scenarios for CBF model

Pulse Type	Scenario	Story	Performance level								Total Braces	
			Elastic (A–B)		IO (B-C)		LS (C-D)		CP (D-E)			
			4-F	8-F	4-F	8-F	4-F	8-F	4-F	8-F	4-F	8-F
Small pulse	NFS1	1st	8	8	8	0	0	0	0	8	64	128
		2nd	8	8	8	0	0	0	0	8	64	128
		3rd	16	8	0	0	0	0	0	8	64	128
		4th	16	8	0	0	0	0	0	8	64	128
		5th	-	8	-	0	-	6	-	2	-	128
		6th	-	8	-	8	-	0	-	0	-	128
		7th	-	12	-	4	-	0	-	0	-	128
		8th	-	16	-	0	-	0	-	0	-	128
	NFS2	1st	8	8	0	0	0	0	8	8	64	128
		2nd	8	8	0	0	0	0	8	8	64	128
		3rd	8	8	0	0	8	0	0	8	64	128
		4th	16	8	0	0	0	0	0	8	64	128
		5th	-	8	-	0	-	0	-	8	-	128
		6th	-	8	-	0	-	0	-	8	-	128
		7th	-	8	-	8	-	0	-	0	-	128
		8th	-	16	-	0	-	0	-	0	-	128
	NFS3	1st	8	8	8	0	0	0	0	8	64	128
		2nd	8	8	8	0	0	0	0	8	64	128
		3rd	8	8	8	0	0	0	0	8	64	128
		4th	16	8	0	0	0	0	0	8	64	128
		5th	-	8	-	0	-	0	-	8	-	128
		6th	-	8	-	0	-	0	-	8	-	128
		7th	-	8	-	8	-	0	-	0	-	128
		8th	-	16	-	0	-	0	-	0	-	128
	NFS4	1st	8	8	8	0	0	8	0	0	64	128

ARTICLE IN PRESS

		2nd	8	8	8	8	0	0	0	0	64	128
		3rd	16	8	0	8	0	0	0	0	64	128
		4th	16	8	0	8	0	0	0	0	64	128
		5th	-	8	-	8	-	0	-	0	-	128
		6th	-	8	-	8	-	0	-	0	-	128
		7th	-	16	-	0	-	0	-	0	-	128
		8th	-	16	-	0	-	0	-	0	-	128
Medium pulse	NFM1	1st	8	8	8	0	8	0	8	8	64	128
		2nd	8	8	0	0	8	0	0	8	64	128
		3rd	8	8	8	0	0	0	0	8	64	128
		4th	16	8	0	0	0	0	0	8	64	128
		5th	-	8	-	0	-	4	-	4	-	128
		6th	-	8	-	8	-	0	-	0	-	128
		7th	-	10	-	6	-	0	-	0	-	128
		8th	-	16	-	0	-	0	-	0	-	128
	NFM2	1st	8	8	0	0	0	0	8	8	64	128
		2nd	8	8	0	0	0	0	8	8	64	128
		3rd	8	8	0	0	8	0	0	8	64	128
		4th	16	8	0	0	0	0	0	8	64	128
		5th	-	8	-	0	-	0	-	8	-	128
		6th	-	8	-	0	-	0	-	8	-	128
		7th	-	8	-	0	-	2	-	6	-	128
		8th	-	8	-	8	-	0	-	0	-	128
	NFM3	1st	8	8	8	0	8	0	8	8	64	128
		2nd	8	8	0	0	0	0	8	8	64	128
		3rd	8	8	8	0	0	0	0	8	64	128
		4th	16	8	0	0	0	0	0	8	64	128
		5th	-	8	-	0	-	0	-	8	-	128
		6th	-	8	-	0	-	0	-	8	-	128
		7th	-	8	-	8	-	0	-	0	-	128
		8th	-	16	-	0	-	0	-	0	-	128
	NFM4	1st	8	8	0	0	0	0	8	8	64	128
		2nd	8	8	0	0	0	0	8	8	64	128
		3rd	8	8	8	0	0	0	0	8	64	128
		4th	16	8	0	0	0	0	0	8	64	128
		5th	-	8	-	0	-	0	-	8	-	128
		6th	-	8	-	0	-	0	-	8	-	128
		7th	-	8	-	8	-	0	-	0	-	128
		8th	-	16	-	0	-	0	-	0	-	128
Large pulse	NFL1	1st	8	8	0	0	0	0	8	8	64	128
		2nd	8	8	0	0	0	0	8	8	64	128
		3rd	8	8	0	0	8	0	0	8	64	128
		4th	12	8	0	0	4	6	0	0	64	128
		5th	-	8	-	4	-	4	-	0	-	128
		6th	-	8	-	8	-	0	-	0	-	128
		7th	-	12	-	4	-	0	-	0	-	128
		8th	-	16	-	0	-	0	-	0	-	128
	NFL2	1st	8	8	0	0	0	0	8	8	64	128
		2nd	8	8	0	0	0	0	8	8	64	128
		3rd	8	8	4	0	4	0	0	8	64	128
		4th	16	8	0	0	0	0	0	8	64	128
		5th	-	8	-	0	-	8	-	0	-	128
		6th	-	8	-	8	-	0	-	0	-	128
		7th	-	16	-	0	-	0	-	0	-	128
		8th	-	16	-	0	-	0	-	0	-	128
	NFL3	1st	8	8	8	0	0	0	0	8	64	128
		2nd	8	8	8	0	0	0	0	8	64	128
		3rd	8	8	8	0	0	4	0	4	64	128
		4th	16	8	0	2	0	6	0	0	64	128
		5th	-	8	-	8	-	0	-	0	-	128
		6th	-	8	-	8	-	0	-	0	-	128
		7th	-	16	-	0	-	0	-	0	-	128
		8th	-	16	-	0	-	0	-	0	-	128
	NFL4	1st	8	8	8	0	8	0	8	8	8	128
		2nd	8	8	0	0	0	0	8	8	64	128

ARTICLE IN PRESS

ARTICLE IN PRESS

	3rd	8	8	0	0	0	0	8	8	64	128
	4th	8	8	8	0	0	0	0	8	64	128
	5th	-	8	-	0	-	0	-	8	-	128
	6th	-	8	-	0	-	0	-	8	-	128
	7th	-	8	-	0	-	0	-	8	-	128
	8th	-	10	-	6	-	0	-	0	-	128

4. Conclusion

This study investigated the nonlinear seismic response of low-rise (4-story) and mid-rise (8-story) steel buildings equipped with CBFs and EBFs subjected to pulse-type NFGEs. A series of NTHAs was conducted using ground motions categorized as SP, MP, and LP. The evaluation focused on displacement-related performance indicators, including story displacements, IDRs, top-floor displacement time histories, and brace performance states. By comparing building height, bracing system type, and pulse-related record groups, the study provides insight into the response trends observed under the selected pulse-type NFGEs. Based on the analysis results, the following conclusions can be drawn:

- The comparison of the maximum IDR demands showed that the EBF systems consistently developed larger drift demands than the corresponding CBF systems for the selected motions. For the 4-story models, the EBF/CBF maximum IDR ratio ranged from 1.10 to 2.92, corresponding to an increase of approximately 10–191%. For the 8-story models, this ratio ranged from 1.05 to 2.91, corresponding to an increase of approximately 5–191%.
- For the 4-story models, the largest maximum IDR was obtained under the NFL4 record, reaching 0.54% in the CBF system and 1.27% in the EBF system. For the 8-story models, the largest maximum IDR was observed under the NFM2 record, reaching 0.84% in the CBF system and 2.17% in the EBF system. These results indicate that the governing pulse group changes with building height.
- In terms of top-floor displacement, the EBF systems also produced larger demand than the CBF systems. For example, in the 8-story models, the NFM2 record produced top-floor displacements of 10.89 cm in the CBF system and 36.67 cm in the EBF system, corresponding to an increase of approximately 237%. This confirms the higher displacement sensitivity of the more flexible EBF configuration under high-intensity medium-period pulse records.
- The observed response trends indicate that seismic response demands are influenced by the combined effects of building height, bracing system type, pulse intensity, pulse duration, and the pulse-to-structure period ratio (T_p/T_1). As building height increases, T_1 becomes closer to the characteristic pulse periods, which may contribute to a transition from a predominantly stiffness-controlled response toward a more momentum-sensitive response.
- The CBF systems effectively limited global displacement demands due to their higher initial lateral stiffness. However, particularly in the 8-story configuration, drift demands tended to concentrate on fewer lower stories once inelastic behavior initiated. In contrast, the EBF systems developed larger but more distributed deformation demands owing to their lower effective stiffness and ductile link-yielding mechanism.
- The influence of T_p/T_1 on displacement and drift demand was not monotonic. NFL records produced the largest demands in the 4-story models when very large T_p/T_1 ratios coincided with high PGA and PGV values. However, in the 8-story models, the maximum response occurred under NFM records, indicating that pulse amplitude, effective momentum transfer, and timing relative to the structural period may be more influential than pulse-period ratio alone.

ARTICLE IN PRESS

- The statistical evaluation based on mean, standard deviation, and COV values indicates noticeable record-to-record variability within the selected pulse groups. The COV values range from approximately 33% to 77%, showing that the response trends are not uniform across individual records. Therefore, although the mean values support the general trends observed in the analyses, the relatively high COV values confirm that the findings should be interpreted as record-dependent trends within the selected ground-motion set rather than statistically generalized conclusions.

Overall, it should be noted that the conclusions are based on a limited set of twelve pulse-type NFGEs, with four records in each pulse category. Therefore, the observed differences should be interpreted as record-dependent response trends rather than statistically conclusive evidence of the isolated influence of pulse duration or pulse type. In addition, the study is limited to 4- and 8-story steel buildings with inverted V-shaped CBF and EBF configurations; therefore, the findings should not be generalized to all bracing systems, building heights, or structural layouts. Future studies should consider a larger and more diverse ground-motion database, including a wider range of pulse periods, PGV/PGA levels, site conditions, and fault-normal/fault-parallel components. Further research may also extend the comparison to additional building heights, alternative bracing configurations, different link lengths, and other performance indicators such as residual drift, energy dissipation, collapse probability, and fragility functions. Such studies would allow a more statistically robust assessment of the interaction between pulse characteristics, building height, and bracing-system response mechanisms.

Data availability

The datasets generated and analyzed during the current study are available from the corresponding author on reasonable request.

Declaration of interests

The authors declare that they have no known competing financial interests or personal relationships that could have appeared to influence the work reported in this paper.

ARTICLE IN PRESS

Funding

This study has been supported by the Recep Tayyip Erdogan University Development Foundation (Grant number: 02026006010386).

Reference

References

[1] R. Tremblay, "Inelastic seismic response of steel bracing members," *Journal of constructional steel research,* vol. 58, no. 5-8, pp. 665-701, 2002, doi: https://doi.org/10.1016/S0143-974X(01)00104-3.

[2] R. Montuori, E. Nastri, and V. Piluso, "Influence of the bracing scheme on seismic performances of MRF-EBF dual systems," *Journal of Constructional Steel Research,* vol. 132, pp. 179-190, 2017, doi: https://doi.org/10.1016/j.jcsr.2017.01.018.

[3] Y. Khademi and M. Rezaie, "Comparison study of CBFs and EBFs bracing in steel structures with nonlinear time history analysis," *Civil Engineering Journal,* vol. 3, no. 11, pp. 1157-1165, 2017, doi: https://doi.org/10.28991/cej-030945.

[4] S. R. Salimbahrami and M. Naghipour, "Numerical study to evaluate the effect of ductile element in the seismic performance of steel frames with EBF," *International Journal of Steel Structures,* vol. 21, no. 2, pp. 549-560, 2021, doi: https://doi.org/10.1007/s13296-021-00455-4.

[5] E. Bakhshivand, H. Ahmadie Amiri, and S. Maleki, "Evaluation of seismic performance factors for dual steel SMF-SCBF systems using FEMA P695 methodology," *Soil Dynamics and Earthquake Engineering,* vol. 163, p. 107506, 2022/12/01/ 2022, doi: https://doi.org/10.1016/j.soildyn.2022.107506.

ARTICLE IN PRESS

[6] S. K. Azad and C. Topkaya, "A review of research on steel eccentrically braced frames," *Journal of constructional steel research,* vol. 128, pp. 53-73, 2017, doi: https://doi.org/10.1016/j.jcsr.2016.07.032.
[7] *Turkish Earthquake Building Code, Specifications for buildings to be built in seismic areas,Ministry of Public Works and Settlement, Ankara,Turkey*, TBEC, 2018.
[8] B. M. Broderick and J. Hickey, "Performance based design of concentrically braced frames using rapid performance assessment methods," presented at the The 17th World Conference on Earthquake Engineering, Sendai, Japan, September 13th to 18th, 2020.
[9] M. A. Q. Al-Janabi and C. Topkaya, "Seismic performance of eccentrically braced frames designed to AISC341 and EC8 specifications," *Structures,* vol. 29, pp. 339-359, 2021 2021, doi: https://doi.org/10.1016/j.istruc.2020.11.031.
[10] Z. Tonyali, "Energy-based optimization of short-link EBFs under pulse-type ground motions using the concept of Uniform Damage Distribution (UDD)," in *Structures*, 2025, vol. 81: Elsevier, p. 110171, doi: https://doi.org/10.1016/j.istruc.2025.110171.
[11] P. P. Rossi and A. Lombardo, "Influence of the link overstrength factor on the seismic behaviour of eccentrically braced frames," *Journal of Constructional Steel Research,* vol. 63, no. 11, pp. 1529-1545, 2007, doi: https://doi.org/10.1016/j.jcsr.2007.01.006.
[12] M. M. Hassan, "State-of-the-art review: Reduction factor of traditional steel moment resisting, braced or eccentrically braced systems," *Structures,* vol. 35, pp. 734-747, 2022 2022, doi: https://doi.org/10.1016/j.istruc.2021.11.028.
[13] Eurocode 8, "Design of structures for earthquake resistance," *Part,* vol. 1, pp. 1998-1, 2005.
[14] E. P. Popov, K. Kasai, and M. D. Engelhardt, "Advances in design of eccentrically braced frames," *Earthquake Spectra,* vol. 3, no. 1, pp. 43-55, 1987.
[15] N. A. Khan and A. Bilal, "Seismic performance evaluation of eccentrically braced steel frame buildings," *Sigma Journal of Engineering and Natural Sciences,* vol. 41, no. 6, pp. 1121-1131, 2023, doi: https://doi.org/10.14744/sigma.2023.00075.
[16] Y. O. Özkılıç, E. M. Ün, and C. Topkaya, "Frictional mid-spliced shear links for eccentrically braced frames," *Earthquake Engineering & Structural Dynamics,* vol. 52, no. 15, pp. 5050-5071, 2023, doi: https://doi.org/10.1002/eqe.4001.
[17] Y. O. Özkılıç and C. Topkaya, "Extended end-plate connections for replaceable shear links," *Engineering Structures,* vol. 240, p. 112385, 2021, doi: https://doi.org/10.1016/j.engstruct.2021.112385.
[18] Y. O. Özkılıç, "Optimized stiffener detailing for shear links in eccentrically braced frames," *Steel and Composite Structures, An International Journal,* vol. 39, no. 1, pp. 35-50, 2021.
[19] T. Okazaki and M. D. Engelhardt, "Cyclic loading behavior of EBF links constructed of ASTM A992 steel," *Journal of constructional steel Research,* vol. 63, no. 6, pp. 751-765, 2007.
[20] P. W. Richards and C.-M. Uang, "Testing protocol for short links in eccentrically braced frames," *Journal of Structural Engineering,* vol. 132, no. 8, pp. 1183-1191, 2006, doi: https://doi.org/10.1061/(ASCE)0733-9445(2006)132:8(1183).
[21] M. Mojarad and M. Daei, "Modification factor for reliable design of shear link in EBF subjected to high axial force based on Eurocode 8," *Structures,* vol. 75, p. 108801, 2025/05/01/ 2025, doi: https://doi.org/10.1016/j.istruc.2025.108801.
[22] L. Manganiello, R. Montuori, E. Nastri, and V. Piluso, "The influence of the axial restraint on the overstrength of short links," *Journal of Constructional Steel Research,* vol. 184, p. 106758, 2021/09/01/ 2021, doi: https://doi.org/10.1016/j.jcsr.2021.106758.
[23] G. Almasabha, "Gene expression model to estimate the overstrength ratio of short links," *Structures,* vol. 37, pp. 528-535, 2022, doi: https://doi.org/10.1016/j.istruc.2022.01.030.
[24] *Seismic provisions for structural steel buildings*, AISC, 2002.
[25] R. Chalabi, O. Yazdanpanah, and K. M. Dolatshahi, "Nonmodel rapid seismic assessment of eccentrically braced frames incorporating masonry infills using machine learning techniques," *Journal of Building Engineering,* vol. 79, p. 107784, 2023/11/15/ 2023, doi: https://doi.org/10.1016/j.jobe.2023.107784.
[26] S. Zhang and G. Wang, "Effects of near-fault and far-fault ground motions on nonlinear dynamic response and seismic damage of concrete gravity dams," *Soil Dynamics and Earthquake Engineering,* vol. 53, pp. 217-229, 2013/10/01/ 2013, doi: https://doi.org/10.1016/j.soildyn.2013.07.014.
[27] M. Davoodi, M. K. Jafari, and N. Hadiani, "Seismic response of embankment dams under near-fault and far-field ground motion excitation," *Engineering Geology,* vol. 158, pp. 66-76, 2013/05/24/ 2013, doi: https://doi.org/10.1016/j.enggeo.2013.02.008.

ARTICLE IN PRESS

ARTICLE IN PRESS

[28] A. K. Chopra and C. Chintanapakdee, "Comparing response of SDF systems to near-fault and far-fault earthquake motions in the context of spectral regions," *Earthquake engineering & structural dynamics,* vol. 30, no. 12, pp. 1769-1789, 2001, doi: https://doi.org/10.1002/eqe.92.

[29] A. Bayraktar, A. C. Altunişik, B. Sevim, M. E. Kartal, T. Türker, and Y. Bilici, "Comparison of near- and far-fault ground motion effect on the nonlinear response of dam–reservoir–foundation systems," *Nonlinear Dynamics,* vol. 58, no. 4, pp. 655-673, 2009/12/01 2009, doi: https://doi.org/10.1007/s11071-009-9508-x.

[30] S. Adanur, A. C. Altunişik, A. Bayraktar, and M. Akköse, "Comparison of near-fault and far-fault ground motion effects on geometrically nonlinear earthquake behavior of suspension bridges," *Natural Hazards,* vol. 64, no. 1, pp. 593-614, 2012/10/01 2012, doi: https://doi.org/10.1007/s11069-012-0259-5.

[31] L. Han and Z. Tao, "Structural performance-based anomaly detection for velocity pulse," *Computer-Aided Civil and Infrastructure Engineering,* vol. 39, no. 12, pp. 1851-1867, 2024, doi: https://doi.org/10.1111/mice.13174.

[32] H. Masaeli, F. Khoshnoudian, and R. Ziaei, "Rocking soil-structure systems subjected to near-fault pulses," *Journal of Earthquake Engineering,* vol. 19, no. 3, pp. 461-479, 2015, doi: https://doi.org/10.1080/13632469.2014.990652.

[33] M. Paredes, T. Wierzbicki, and C. C. Roth, "Three dimensional, flexural-torsional dynamic buckling of long wires after tensile fracture and implications on deep water riser dynamics," *International Journal of Impact Engineering,* vol. 86, pp. 27-39, 2015, doi: https://doi.org/10.1016/j.ijimpeng.2015.07.004.

[34] Z. Chang, H. Wu, and K. Goda, "Automated parameterization of velocity pulses in near-fault ground motions," *Earthquake Engineering & Structural Dynamics,* vol. 53, no. 3, pp. 1006-1027, 2024, doi: https://doi.org/10.1002/eqe.4053.

[35] E. Chioccarelli and I. Iervolino, "Near-source seismic demand and pulse-like records: A discussion for L'Aquila earthquake," *Earthquake Engineering & Structural Dynamics,* vol. 39, no. 9, pp. 1039-1062, 2010, doi: https://doi.org/10.1002/eqe.987.

[36] W.-P. Wen, C.-H. Zhai, S. Li, Z. Chang, and L.-L. Xie, "Constant damage inelastic displacement ratios for the near-fault pulse-like ground motions," *Engineering structures,* vol. 59, pp. 599-607, 2014, doi: https://doi.org/10.1016/j.engstruct.2013.11.011.

[37] Y. R. Dong *et al.*, "Experimental study and multi-scale refinement model of high damping acrylic polymer matrix VEDs for civil structural seismic retrofit," *Earthquake Engineering & Structural Dynamics,* vol. 53, no. 9, pp. 2908-2928, 2024, doi: https://doi.org/10.1002/eqe.4147.

[38] M. Zhao, C. Zhang, X. Li, and N. Zhai, "Dynamic Responses of Concrete-Face Rockfill Dam to Different Site Conditions under Near-Fault Earthquake Excitation," *Buildings,* vol. 13, no. 10, p. 2410, 2023, doi: https://doi.org/10.3390/buildings13102410.

[39] C. Fang, Q. Zhong, W. Wang, S. Hu, and C. Qiu, "Peak and residual responses of steel moment-resisting and braced frames under pulse-like near-fault earthquakes," *Engineering structures,* vol. 177, pp. 579-597, 2018, doi: https://doi.org/10.1016/j.engstruct.2018.10.013.

[40] Z. Tonyali, M. Yurdakul, and H. Sesli, "Dynamic Response of Concentrically Braced Steel Frames to Pulse Period in Near-Fault Ground Motions," *Turkish Journal of Science and Technology,* vol. 17, no. 2, pp. 357-373, 2022, doi: https://doi.org/10.55525/tjst.1113021.

[41] Z. Zhao, W. Zhang, Y. Ding, and H. Li, "Effects of Reserve Capacity on Seismic Response of Concentrically Braced Frames by Considering Brace Failure," *Materials,* vol. 15, no. 13, p. 4377, 2022, doi: https://doi.org/10.3390/ma15134377.

[42] M. Dicleli and A. Mehta, "Effect of near-fault ground motion and damper characteristics on the seismic performance of chevron braced steel frames," *Earthquake engineering & structural dynamics,* vol. 36, no. 7, pp. 927-948, 2007, doi: https://doi.org/10.1002/eqe.662.

[43] H. J. He, X. L. Cao, and J. P. Hao, "Research on the Seismic Behaviors of Link Beam for Eccentrically Braced Low Yield Point Steel Frames," *Applied Mechanics and Materials,* vol. 201, pp. 185-188, 2012, doi: https://doi.org/10.4028/www.scientific.net/AMM.201-202.185.

[44] K. Ma, X. Ye, R. Wu, H. Yu, Y. Wu, and L. Jiang, "Seismic performance assessment of eccentrically braced steel frames with variable-cross-section horizontal shear links," *Advances in Structural Engineering,* vol. 25, no. 10, pp. 2089-2102, 2022, doi: https://doi.org/10.1177/13694332221088944.

[45] B. C. Zhao and Q. Gu, "Energy-Dissipation Mechanisms and Seismic Design Recommendation of Eccentrically Braced Steel Frames," *Applied Mechanics and Materials,* vol. 71, pp. 3662-3665, 2011, doi: https://doi.org/10.4028/www.scientific.net/AMM.71-78.3662.

ARTICLE IN PRESS

[46] R. Matsui, T. Takeuchi, S. Urui, and M. Tokuno, "Collapse analysis of steel frames considering fracture of braces and end of beams," *Key Engineering Materials,* vol. 763, pp. 686-693, 2018, doi: https://doi.org/10.4028/www.scientific.net/KEM.763.686.

[47] K. Karsaz and S. V. R. Tosee, "A comparative study on the behavior of steel moment-resisting frames with different bracing systems based on a response-based damage index," *Civil Engineering Journal,* vol. 4, no. 6, pp. 1354-1373, 2018, doi: https://doi.org/10.28991/cej-0309178.

[48] A. J. Abdulridha, "Behavior of a Multi-Story Steel Structure with Eccentric X-Brace," *Fracture & Structural Integrity/Frattura ed Integrità Strutturale,* no. 66, 2023, doi: https://doi.org/10.3221/IGF-ESIS.66.17.

[49] Y. Hu, J. S. Lei, and W. X. Luo, "Analyses in Seismic Responses of Different Types of Eccentrically Braced Steel Frames," *Advanced Materials Research,* vol. 243, pp. 3737-3742, 2011, doi: https://doi.org/10.4028/www.scientific.net/AMR.243-249.3737.

[50] Y.-P. Wu, Z.-H. Chen, T. Zhou, X.-D. Chen, and X.-D. Wang, "Experimental and numerical studies on Seismic Performance of The SCFST Column Eccentrically Braced Frames," *Advances in Structural Engineering,* vol. 24, no. 2, pp. 266-278, 2021, doi: https://doi.org/10.1177/1369433220950609.

[51] A. Rouhi and H. Hamidi, "Development of performance based plastic design of EBF steel structures subjected to forward directivity effect," *International Journal of Steel Structures,* vol. 21, no. 3, pp. 1092-1107, 2021, doi: https://doi.org/10.1007/s13296-021-00491-0.

[52] S. Etli and E. M. Güneyisi, "Effect of Using Eccentric Braces with Different Link Lengths on the Seismic Demand of CFST Column-Composite Beam Frames Subjected to Near-Field and Far-Field Earthquakes," *Iranian Journal of Science and Technology, Transactions of Civil Engineering,* vol. 47, no. 3, pp. 1599-1627, 2023/06/01 2023, doi: https://doi.org/10.1007/s40996-022-00994-8.

[53] H. Azizi and J. Ahmadi, "Mitigation of residual deformations in steel braced frames through an innovative Y-shaped hybrid buckling restrained braces," *Journal of Constructional Steel Research,* vol. 229, p. 109533, 2025, doi: https://doi.org/10.1016/j.jcsr.2025.109533.

[54] H. Azizi, J. Ahmadi, and M. Eghbali, "Study on self-centering mechanism of different yield strength hybrid buckling restrained braces," *Journal of Constructional Steel Research,* vol. 210, p. 108068, 2023, doi: https://doi.org/10.1016/j.jcsr.2023.108068.

[55] H. Azizi, J. Ahmadi, and K. Nasserasadi, "Seismic performance of double-stage yield buckling restrained braced frames under mainshock-aftershock sequences," *Journal of Building Engineering,* vol. 111, p. 113141, 2025, doi: https://doi.org/10.1016/j.jobe.2025.113141.

[56] K. Soyluk and H. Karaca, "Near-fault and far-fault ground motion effects on cable-supported bridges," *Procedia engineering,* vol. 199, pp. 3077-3082, 2017, doi: https://doi.org/10.1016/j.proeng.2017.09.421.

[57] S. Mahmoud, A. Alqarni, J. Saliba, A. H. Ibrahim, M. genidy, and H. Diab, "Influence of floor system on seismic behavior of RC buildings to forward directivity and fling-step in the near-fault region," *Structures,* vol. 30, pp. 803-817, 2021/04/01/ 2021, doi: https://doi.org/10.1016/j.istruc.2021.01.052.

[58] P. G. Somerville, "Magnitude scaling of the near fault rupture directivity pulse," *Physics of the Earth and Planetary Interiors,* vol. 137, no. 1, pp. 201-212, 2003/05/15/ 2003, doi: https://doi.org/10.1016/S0031-9201(03)00015-3.

[59] A. Ghobarah, "Response of structures to near-fault ground motion," in *13th World Conference on Earthquake Engineering*, Vancouver, British Columbia, Canada,, August 1-6 2004, vol. 1031.

[60] B. Halldórsson, G. P. Mavroeidis, and A. S. Papageorgiou, "Near-fault and far-field strong ground-motion simulation for earthquake engineering applications using the specific barrier model," *Journal of Structural Engineering,* vol. 137, no. 3, pp. 433-444, 2011, doi: https://doi.org/10.1061/(ASCE)ST.1943-541X.0000097.

[61] J. D. Bray and A. Rodriguez-Marek, "Characterization of forward-directivity ground motions in the near-fault region," *Soil dynamics and earthquake engineering,* vol. 24, no. 11, pp. 815-828, 2004, doi: https://doi.org/10.1016/j.soildyn.2004.05.001.

[62] J. L. Gillie, A. Rodriguez-Marek, and C. McDaniel, "Strength reduction factors for near-fault forward-directivity ground motions," *Engineering Structures,* vol. 32, no. 1, pp. 273-285, 2010/01/01/ 2010, doi: https://doi.org/10.1016/j.engstruct.2009.09.014.

[63] M. Ismail, J. R. Casas, and J. Rodellar, "Near-fault isolation of cable-stayed bridges using RNC isolator," *Engineering structures,* vol. 56, pp. 327-342, 2013, doi: https://doi.org/10.1016/j.engstruct.2013.04.007.

[64] M. Kohrangi, D. Vamvatsikos, and P. Bazzurro, "Pulse-like versus non-pulse-like ground motion records: spectral shape comparisons and record selection strategies," *Earthquake Engineering & Structural Dynamics,* vol. 48, no. 1, pp. 46-64, 2019, doi: https://doi.org/10.1002/eqe.3122.

ARTICLE IN PRESS

ARTICLE IN PRESS

[65] P. G. Somerville, N. F. Smith, R. W. Graves, and N. A. Abrahamson, "Modification of empirical strong ground motion attenuation relations to include the amplitude and duration effects of rupture directivity," *Seismological research letters,* vol. 68, no. 1, pp. 199-222, 1997, doi: https://doi.org/10.1785/gssrl.68.1.199.

[66] P. K. Malhotra, "Response of buildings to near-field pulse-like ground motions," *Earthquake engineering & structural dynamics,* vol. 28, no. 11, pp. 1309-1326, 1999, doi: https://doi.org/10.1002/(SICI)1096-9845(199911)28:11%3C1309::AID-EQE868%3E3.0.CO;2-U.

[67] G. P. Mavroeidis, G. Dong, and A. S. Papageorgiou, "Near-fault ground motions, and the response of elastic and inelastic single-degree-of-freedom (SDOF) systems," *Earthquake Engineering & Structural Dynamics,* vol. 33, no. 9, pp. 1023-1049, 2004, doi: https://doi.org/10.1002/eqe.391.

[68] S. K. Shahi and J. W. Baker, "An empirically calibrated framework for including the effects of near-fault directivity in probabilistic seismic hazard analysis," *Bulletin of the Seismological Society of America,* vol. 101, no. 2, pp. 742-755, 2011, doi: https://doi.org/10.1785/0120100090.

[69] G. Baltzopoulos, L. Luzi, and I. Iervolino, "Analysis of Near-Source Ground Motion from the 2019 Ridgecrest Earthquake Sequence," *Bulletin of the Seismological Society of America,* vol. 110, no. 4, pp. 1495-1505, 2020, doi: https://doi.org/10.1785/0120200038.

[70] M. H. Yen, S. von Specht, Y. Y. Lin, F. Cotton, and K. F. Ma, "Within- and Between-Event Variabilities of Strong-Velocity Pulses of Moderate Earthquakes within Dense Seismic Arrays," *Bulletin of the Seismological Society of America,* vol. 112, no. 1, pp. 361-380, 2021, doi: https://doi.org/10.1785/0120200376.

[71] R. Sehhati, A. Rodriguez-Marek, M. ElGawady, and W. F. Cofer, "Effects of near-fault ground motions and equivalent pulses on multi-story structures," *Engineering Structures,* vol. 33, no. 3, pp. 767-779, 2011/03/01/ 2011, doi: https://doi.org/10.1016/j.engstruct.2010.11.032.

[72] J. W. Baker, "Quantitative Classification of Near-Fault Ground Motions Using Wavelet Analysis," *Bulletin of the Seismological Society of America,* vol. 97, no. 5, pp. 1486-1501, 2007, doi: https://doi.org/10.1785/0120060255.

[73] D. Yang, J. Pan, and G. Li, "Interstory drift ratio of building structures subjected to near-fault ground motions based on generalized drift spectral analysis," *Soil Dynamics and Earthquake Engineering,* vol. 30, no. 11, pp. 1182-1197, 2010, doi: https://doi.org/10.1016/j.soildyn.2010.04.026.

[74] W.-I. Liao, C.-H. Loh, and B.-H. Lee, "Comparison of dynamic response of isolated and non-isolated continuous girder bridges subjected to near-fault ground motions," *Engineering Structures,* vol. 26, no. 14, pp. 2173-2183, 2004/12/01/ 2004, doi: https://doi.org/10.1016/j.engstruct.2004.07.016.

[75] B. Alavi and H. Krawinkler, "Behavior of moment-resisting frame structures subjected to near-fault ground motions," *Earthquake engineering & structural dynamics,* vol. 33, no. 6, pp. 687-706, 2004, doi: https://doi.org/10.1002/eqe.369.

[76] N. Güneş and Z. Ç. Ulucan, "Nonlinear dynamic response of a tall building to near-fault pulse-like ground motions," *Bulletin of Earthquake Engineering,* vol. 17, no. 6, pp. 2989-3013, 2019/06/01 2019, doi: https://doi.org/10.1007/s10518-019-00570-y.

[77] PEER. Ground motions Database Pacific Earthquake Engineering Research Center. University of California, California [Online] Available: https://ngawest2.berkeley.edu/

[78] *Seismosoft, Earthquake Engineering Software Products, V2024*. (2024). [Online]. Available: https://seismosoft.com

[79] V. Kardoutsou, I. Taflampas, and I. N. Psycharis, "A new pulse indicator for the classification of ground motions," *Bulletin of the Seismological Society of America,* vol. 107, no. 3, pp. 1356-1364, 2017, doi: https://doi.org/10.1785/0120160301.

[80] K. Kasai and E. P. Popov, "General behavior of WF steel shear link beams," *Journal of Structural Engineering,* vol. 112, no. 2, pp. 362-382, 1986.

[81] M. Bosco, E. M. Marino, and P. P. Rossi, "Modelling of steel link beams of short, intermediate or long length," *Engineering structures,* vol. 84, pp. 406-418, 2015, doi: https://doi.org/10.1016/j.engstruct.2014.12.003.

[82] M. Bosco and P. P. Rossi, "Seismic behaviour of eccentrically braced frames," *Engineering Structures,* vol. 31, no. 3, pp. 664-674, 2009, doi: https://doi.org/10.1016/j.engstruct.2008.11.002.

[83] M. Lian, M. Su, and Y. Guo, "Seismic performance of eccentrically braced frames with high strength steel combination," *Steel and Composite Structures,* vol. 18, no. 6, pp. 1517-1539, 2015, doi: https://doi.org/10.12989/scs.2015.18.6.1517.

[84] J. M. Ricles and E. P. Popov, *Experiments on eccentrically braced frames with composite floors*. Earthquake Engineering Research Center, University of California Berkeley …, 1987.

ARTICLE IN PRESS

[85] M. G. Vetr, A. Ghamari, and J. Bouwkamp, "Investigating the nonlinear behavior of Eccentrically Braced Frame with vertical shear links (V-EBF)," *Journal of Building Engineering,* vol. 10, pp. 47-59, 2017/03/01/ 2017, doi: https://doi.org/10.1016/j.jobe.2017.02.002.
[86] A. Daneshmand and B. Hosseini Hashemi, "Performance of intermediate and long links in eccentrically braced frames," *Journal of Constructional Steel Research,* vol. 70, pp. 167-176, 2012/03/01/ 2012, doi: https://doi.org/10.1016/j.jcsr.2011.10.011.
[87] C. W. Roeder and E. P. Popov, "Inelastic behavior of eccentrically braced steel frames under cyclic loadings," *NASA STI/recon technical report N,* vol. 78, p. 20375, 1977.
[88] K. D. Hjelmstad and E. P. Popov, "Cyclic behavior and design of link beams," *Journal of Structural Engineering,* vol. 109, no. 10, pp. 2387-2403, 1983.
[89] FEMA-356, "Prestandard and commentary for the seismic rehabilitation of buildings," *Federal Emergency Management Agency: Washington, DC, USA,* 2000.
[90] *Seismic Provisions for Structural Steel Buildings (ANSI/AISC 341-16)*, AISC, American Institute of Steel Construction, 2016.
[91] P. Uriz, *Toward earthquake-resistant design of concentrically braced steel-frame structures*. Pacific Earthquake Engineering Research Center, 2008.
[92] A. C. Salmasi and M. R. Sheidaii, "Assessment of eccentrically braced frames strength against progressive collapse," *International Journal of Steel Structures,* vol. 17, no. 2, pp. 543-551, 2017, doi: https://doi.org/10.1007/s13296-017-6014-8.
[93] N. Zandi, M. R. Adlparvar, and A. Lamei Javan, "Evaluation on Seismic Performance of Dual Steel Moment-Resisting Frame with Zipper Bracing System Compared to Chevron Bracing System Against Near-Fault Earthquakes," *Journal of Rehabilitation in Civil Engineering,* vol. 9, no. 3, pp. 1-25, 2021, doi: https://doi.org/10.22075/JRCE.2021.20562.1426.
[94] M. D'Aniello, G. L. M. Ambrosino, F. Portioli, and R. Landolfo, "Modelling aspects of the seismic response of steel concentric braced frames," *Steel and Composite Structures,* vol. 15, no. 5, pp. 539-566, 2013, doi: https://doi.org/10.12989/scs.2013.15.5.539.
[95] C. S. T. Leader *et al.*, "Tri-Axial Hinge Knee Brace," 2015.
[96] S. Costanzo, "State of the Art on Seismic Design of Steel Buildings in Europe," *Buildings,* vol. 13, no. 6, p. 1563, 2023, doi: https://doi.org/10.3390/buildings13061563.
[97] M. D'Aniello, S. Costanzo, and R. Landolfo, "The influence of beam stiffness on seismic response of chevron concentric bracings," *Journal of Constructional Steel Research,* vol. 112, pp. 305-324, 2015, doi: https://doi.org/10.1016/j.jcsr.2015.05.021.
[98] S. Costanzo and L. Raffaele, "Concentrically Braced Frames: European vs. North American Seismic Design Provisions," *The Open Civil Engineering Journal,* vol. 11, pp. 453-463, 2017, doi: https://doi.org/10.2174/1874149501711010453.
[99] V. Mohsenian, R. Filizadeh, I. Hajirasouliha, and R. Garcia, "Seismic performance assessment of eccentrically braced steel frames with energy-absorbing links under sequential earthquakes," *Journal of Building Engineering,* vol. 33, p. 101576, 2021, doi: https://doi.org/10.1016/j.jobe.2020.101576.

ARTICLE IN PRESS